

AD-A112 431

NAVAL POSTGRADUATE SCHOOL MONTEREY CA  
20 KHZ ACOUSTIC FLUCTUATIONS DUE TO THERMAL FINESTRUCTURE IN TH--ETC(U)  
DEC 81 M WAKEMAN

F/G 20/1

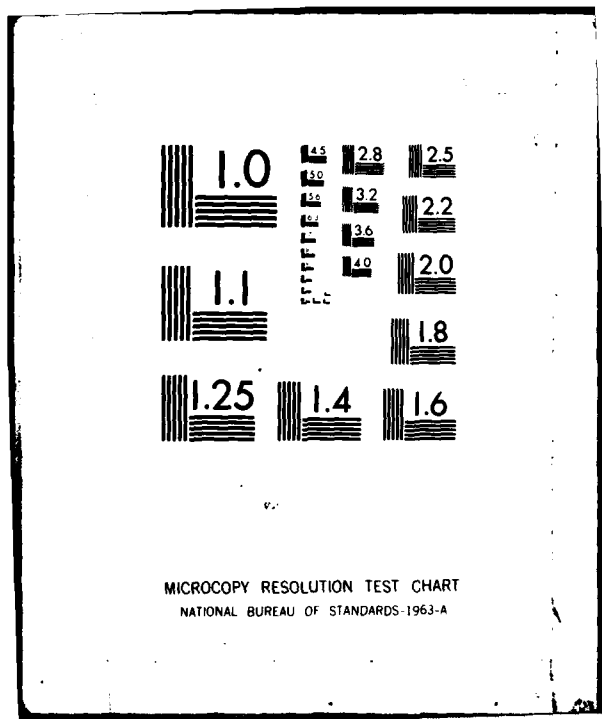
UNCLASSIFIED

NL

1-1  
2000

1-1

END  
DATE  
FILMED  
4 82  
DTIC



MICROCOPY RESOLUTION TEST CHART  
NATIONAL BUREAU OF STANDARDS-1963-A

2

AD A 1 1 2 4 3 1

# NAVAL POSTGRADUATE SCHOOL Monterey, California



## THESIS

20 KHZ ACOUSTIC FLUCTUATIONS DUE TO  
THERMAL FINESTRUCTURE IN THE UPPER OCEAN

by

Mark Wakeman

December 1981

Thesis Advisor:

E. B. Thornton

Approved for public release; distribution unlimited.

SECRET  
MAR 22 1982  
A

DTIC FILE COPY

82 03 92 03H

UNCLASSIFIED

SECURITY CLASSIFICATION OF THIS PAGE (When Data Entered)

REPORT DOCUMENTATION PAGE		READ INSTRUCTIONS BEFORE COMPLETING FORM
1. REPORT NUMBER	2. GOVT ACCESSION NO.	3. RECIPIENT'S CATALOG NUMBER
4. TITLE (and Subtitle) 20 KHz Acoustic Fluctuations Due to Thermal Finestructure in the Upper Ocean		5. TYPE OF REPORT & PERIOD COVERED Master's Thesis; December 1981
7. AUTHOR(s) Mark Wakeman		6. PERFORMING ORG. REPORT NUMBER
8. PERFORMING ORGANIZATION NAME AND ADDRESS Naval Postgraduate School Monterey, California 93940		9. CONTRACT OR GRANT NUMBER(s)
11. CONTROLLING OFFICE NAME AND ADDRESS Naval Postgraduate School Monterey, California 93940		10. PROGRAM ELEMENT, PROJECT, TASK AREA & WORK UNIT NUMBERS
14. MONITORING AGENCY NAME & ADDRESS (if different from Controlling Office)		12. REPORT DATE December 1981
		13. NUMBER OF PAGES 85
		15. SECURITY CLASS. (of this report) Unclassified
		15a. DECLASSIFICATION/DOWNGRADING SCHEDULE
16. DISTRIBUTION STATEMENT (of this Report) Approved for public release; distribution unlimited.		
17. DISTRIBUTION STATEMENT (of the abstract entered in Block 20, if different from Report)		
18. SUPPLEMENTARY NOTES		
19. KEY WORDS (Continue on reverse side if necessary and identify by block number) Acoustic Variability Experiment (AVEX) Thermal Fine Structure 20 KHz Acoustic Fluctuations		
20. ABSTRACT (Continue on reverse side if necessary and identify by block number) The Acoustic Variability Experiment (AVEX) described here measured acoustic pulses which travel a wholly refracted (400m) path between a source and receiver in the upper ocean. The 20 KHz pulse travel times had rms variations between 1 and 60 microseconds, calculated over each half hour sample period, and corresponding pulse amplitude fluctuations between 3% and 14%.		

DD FORM 1473  
1 JAN 73

EDITION OF 1 NOV 68 IS OBSOLETE  
S/N 0102-014-6601

UNCLASSIFIED

SECURITY CLASSIFICATION OF THIS PAGE (When Data Entered)

UNCLASSIFIED

SECURITY CLASSIFICATION OF THIS PAGE/When Data Entered

#20 - ABSTRACT - (CONTINUED)

The temporal and spatial structure of the temperature field were measured simultaneously with the acoustic transmission. A spectrum of a 15-day temperature record showed the presence of inertial and tidal motions, and internal waves at higher frequencies. Microstructure was intermittent and appeared to be associated with internal waves. The temperature integral scales calculated from the spatial autocorrelation functions ranged from 1.2 to 14m (est) in the vertical and from 3.4m to greater than 50m (est) in the horizontal. The temperature structure was anisotropic with the average horizontal to vertical scale ratio equal to about four. A comparison of the measured acoustic amplitude variance with temperature variance and scale lengths measured at the receiver station showed poor correlation using the theoretical models of Chernov and Debye.



SEARCHED	<input checked="" type="checkbox"/>
SERIALIZED	<input type="checkbox"/>
INDEXED	<input type="checkbox"/>
FILED	<input type="checkbox"/>
JAN 1973	
DTIC	
COPY	
INSPECTED	
2	
A	

Approved for public release; distribution unlimited.

20KHz Acoustic Fluctuations Due to  
Thermal Finestructure in the Upper Ocean

by

Mark Wakeman  
Lieutenant Commander, United States Navy  
B.S., Florida Atlantic University, 1970

Submitted in partial fulfillment of the  
requirements for the degree of

MASTER OF SCIENCE IN OCEANOGRAPHY

from the

NAVAL POSTGRADUATE SCHOOL

December 1981

Author

Mark Wakeman

Approved by:

Edward B. Thornton

Thesis Advisor

Tim Stanton

Co-Advisor

William M. Collier  
Chairman, Department of Oceanography

William M. Collier  
Dean of Science and Engineering

## ABSTRACT

The Acoustic Variability Experiment (~~AVEX~~) described here measured acoustic pulses which travel a wholly refracted (400m) path between a source and receiver in the upper ocean. The 20 KHz pulse travel times had rms variations between 1 and 60 microseconds, calculated over each half hour sample period, and corresponding pulse amplitude fluctuations between 3% and 14%.

The temporal and spatial structure of the temperature field were measured simultaneously with the acoustic transmission. A spectrum of a 15-day temperature record showed the presence of inertial and tidal motions, and internal waves at higher frequencies. Microstructure was intermittent and appeared to be associated with internal waves. The temperature integral scales calculated from the spatial autocorrelation functions ranged from 1.2 to 14m (est) in the vertical and from 3.4m to greater than 50m (est) in the horizontal. The temperature structure was anisotropic with the average horizontal to vertical scale ratio equal to about four. A comparison of the measured acoustic amplitude variance with temperature variance and scale lengths measured at the receiver station showed poor correlation using the theoretical models of Chernov and Debye.

TABLE OF CONTENTS

I.	INTRODUCTION -----	9
II.	LITERATURE REVIEW -----	11
	A. MICROSTRUCTURE -----	12
	B. ACOUSTIC PROPAGATION -----	17
	C. ACOUSTIC PROPAGATION EXPERIMENTS -----	24
III.	ACOUSTIC VARIABILITY EXPERIMENT (AVEX) -----	29
	A. EXPERIMENT DESCRIPTION -----	29
	1. Station T -----	29
	2. Station R -----	35
	3. Station P -----	39
	4. Current Meter Array -----	39
	5. Shore Station -----	40
	B. INSTRUMENTATION -----	40
	C. PROCEDURE -----	44
	D. DATA PROCESSING -----	49
IV.	DATA ANALYSIS -----	52
V.	SUMMARY AND CONCLUSIONS -----	79
	LIST OF REFERENCES -----	81
	INITIAL DISTRIBUTION LIST -----	84

LIST OF TABLES

I.	Thermistor Array Spacings -----	38
II.	Instrument Summary -----	42

## LIST OF FIGURES

### Figure

1.	Regimes of $\Lambda$ - $\phi$ Space -----	25
2.	Schematic Cross-section of Experimental Location -----	30
3.	Plan View of Experiment Layout -----	31
4.	Fathometer Trace Across Carmel Canyon -----	32
5.	Transmitter Tower Schematic -----	33
6.	Photograph of Transmitter Tower -----	34
7.	Receiver Tower Schematic -----	36
8.	Photograph of Receiver Tower -----	37
9.	Photograph of Shore Station -----	41
10.	Current Wave Form of the Composite Signal Pulse (upper panel), and Voltage Wave Form of the Composite Signal Pulse (lower panel) ---	45
11.	Data Acquisition and Real Time Processing Schematic -----	48
12.	Temperature, Current Direction and Speed and Tidal Elevation Measured Using 46m Depth Aanderra Current Meter in Carmel Canyon -----	53
13.	Spectrum of Temperature Fluctuations at 46m Depth in Carmel Canyon, 5-23 August 1979 -----	55
14.	25 Minute Environmental Data Records Starting 0100 Hours, 17 August -----	56
15.	25 Minute Environmental Data Records Starting 0300 Hours, 17 August -----	57
16.	25 Minute Environmental Data Records Starting 0700 Hours, 17 August -----	58
17.	25 Minute Environmental Data Records Starting 0900 Hours, 17 August -----	59

18.	Vertical Array Structure Functions (top row) and Autocorrelation Functions (second row), and Horizontal Array Structure Functions (third row) and Autocorrelation Functions (bottom row) for 0100 (left column) and 0300 (right column) 17 August -----	62
19.	Vertical Array Structure Functions (top row) and Autocorrelation Functions (second row), and Horizontal Array Structure Functions (third row) and Autocorrelation Functions (bottom row) for 0100 (left column) and 0300 (right column) 17 August -----	63
20.	Travel-time Estimates for August 16, Hours 1, 3, 5, 7, and 19 -----	66
21.	Time-series of Standard Deviations of Travel- time and Pulse Amplitude for August 16-18 -----	67
22.	20KHz Pulse Amplitude for August 16, Hours 1, 3, 5, 7 and 19 -----	69
23.	Correlation Plot of Travel-time, $\sigma_{tt}$ , and Pulse Amplitude, $\sigma_I$ , Standard Deviations -----	70
24.	Strength, $\phi$ , versus Diffraction, $\Lambda$ , for 16-18 August, using Vertical Length Scales Measured at the Receiver Tripod -----	72
25.	Strength, $\phi$ , versus Diffraction, $\Lambda$ , for 16-18 August, using Horizontal Length Scales Measured at the Receiver Tripod -----	73
26.	Horizontal and Vertical Length Scales, Temperature Standard Deviation and Pulse Amplitude Standard Deviation for August 16-18 --	74
27.	Horizontal and Vertical Length Scales, Temperature Standard Deviation and Travel- time Deviation for August 16-18 -----	76
28.	Correlation Between Amplitude Variations, Length-scales and Temperature Variance Using Chernov's Model -----	77
29.	Correlation Between Amplitude Variations, Length-scales and Temperature Variance Using the Debye Approximation -----	78

## I. INTRODUCTION

The Acoustic Variability Experiment (AVEX) described here measured acoustic pulses which travel a wholly refracted (400m) path between source and receiver in the upper ocean. The acoustic pulse was composed of a 0.5ms burst of 20 KHz CW followed by a 4.5ms pseudo random noise pulse containing energy in the frequency range between 5 and 25 KHz. The temporal variability of acoustic amplitude and phase was measured. The temporal and spatial structure of the temperature field was measured simultaneously with the acoustic transmission at the source, receiver and at a mid-point. It is hypothesized that the acoustic variability for 5-25 KHz frequency range signals in the upper ocean is due primarily to variations in the finestructure of the index of refraction as inferred by the temperature, and that the variations in the temperature structure are associated with tides and/or internal waves.

There are a number of acoustic scattering theories (see for example Chernov (1960) and Tatarski (1961)) where the transmission medium is characterized by a correlation length calculated from the correlation function, or by the structure function, of the oceanic index of refraction. The application of these theories assumes stationarity and homogeneity of the statistic describing the index of refraction. There is growing evidence that the ocean finestructure as represented

by temperature fluctuations is not homogeneous or stationary, particularly in the upper ocean (see for example Gibson, 1980). It is expected that the acoustic variability in the upper ocean is not stationary, but episodic, due to non-stationarity of the index of refraction as measured by the temperature structure.

The objectives of this paper are to describe the Acoustic Variability Experiment (AVEX), and to perform a preliminary analysis of the dependence of the acoustic phase and amplitude fluctuations on the measured ocean thermal fine- and microstructure in the upper ocean. AVEX was conducted in Carmel Bay, California during the month of August 1979. Specific measurements during AVEX described here include:

- 1) Amplitude and phase (travel time) fluctuations of a 20 KHz acoustic pulse transmitted from and received by stable, bottom mounted platforms, via a wholly refracted path.
- 2) Temperature finestructure obtained from horizontal and vertical thermistor arrays mounted on the two fixed bottom platforms.
- 3) Waves and currents near the acoustic pulse path, wind speed and direction, solar insolation, and barometric pressure in the experimental area.

## II. LITERATURE REVIEW

Temperature micro- and fine-structure occur in the ocean as patches of thermal inhomogeneity. The inhomogeneities are of various sizes, shapes, and temperatures, which act to focus or defocus the sound waves. The terms microstructure and finestructure refer to measurement scales of a lesser magnitude than the gross temperature structure. Finestructure is generally accepted to reflect vertical structure sizes in the order of meters, while microstructure refers to fluctuations with vertical scales of less than one meter (Federov, 1978). It is necessary to first separately review the microstructure and the acoustics before the connection between the two can be investigated.

The stochastic nature of oceanic turbulence must be described statistically. Three statistical descriptors to be used are: 1) the autocovariance function, 2) the structure function, and 3) the variance spectrum. Each technique requires a statistically homogeneous medium and a certain degree of stationarity.

### 1. Autocovariance Function

The autocovariance function,  $R_x(\rho)$ , is characterized by the mutual relation between the fluctuations at different times and positions in space. It is expressed by

$$R_x(\rho) = E[(T(x)T(x+\rho))] \quad (1)$$

where E indicates expected value and  $\rho$  is the spatial lag or distance between the two sensors.

## 2. Structure Function

The structure function,  $D_x(\rho)$ , is given by

$$D_x(\rho) = E[(T(x) - T(x+\rho))^2] \quad (2)$$

and for a completely stationary process reduces to

$$D_x(\rho) = 2(R_x(0) - R_x(\rho)) \quad (3)$$

## 3. Spectrum

The fourier transform of the autocovariance function is the energy density spectrum describing the variance of the temperature structure in wave number or frequency space. The one-dimensional spectrum in wave number space is given by

$$S_x(k) = \int_0^{\infty} R_x(\rho) e^{-2\pi i k \rho} d\rho \quad (4)$$

### A. MICROSTRUCTURE

A large number of observations of thermal structure have been made in recent years due to the advent of improved instrumentation. The discussion here will be limited to temperature measurements acquired in the upper ocean pertinent to AVEX. Descriptions of upper ocean thermal processes are relatively limited because the considerable complexity

in this region of the ocean does not lend itself to a simple picture.

Observation of the horizontal and vertical ocean temperature profiles have revealed small scale variations from the gross macroscale changes known previously. The microscale inhomogeneities, with scales less than one meter, exist to some extent throughout the oceans, despite the diffusion and mixing processes which tend to obliterate them. Federov (1978) summarized the spatial scales of the finestructure of temperature and salinity. He points out the strong anisotropy, with the average order of the horizontal to vertical length scales on the order 10.

According to Munk (1981), micro or finestructures are due to internal wave straining or intrusive processes. Intrusive processes occur where two different water masses intersect with resulting interleaving as, for example, occurs at a front. The finestructure is identified by layering of intense temperature inversions which are generally balanced by positive salinity gradients, so that density increases stably with depth. When finestructure laminae of water of differing salinity and temperature occur, microstructure can result due to "fingering" by double diffusion (Turner, 1981). Because of the water mass structure of Carmel Bay, we would not normally expect intrusive processes to be important in AVEX. However this would not be true in winter when the Carmel River discharges fresh water into the Bay.

The more commonly observed (Woods, 1968) or inferred mechanism for microstructure generation is due to internal waves. The occurrence of internal wave breaking has been characterized by Munk (1981) as analogous to the intermittent white capping of surface waves in a light wind. The intermittent, or episodic nature, of breaking internal waves results in the observed patchiness of microstructure. Because internal wave breaking is episodic, the relatively high frequency induced temperature fluctuations are nonstationary over time (length) scales of the order of several internal wave periods (lengths).

Munk (1981) gives an interesting summary of the present knowledge of the little understood subject of breaking internal waves. Breaking can apparently be due to either advective instability or shear instability. Advective instability occurs when the water particle speed at the crest exceeds the wave speed, similar to wave breaking on a beach. The breaking condition occurs for large amplitude, or large slope, internal waves, and can occur in the absence of shear, although it is augmented by shear.

The limiting case of shear instability is Kelvin-Helmholtz instability which can occur at an abrupt density transition even in the absence of finite amplitude waves. Munk (1981) provides an argument that, for linear internal waves only in the presence of self-shear, conditions favor advective instability over shear instability, and that the wave field

is within a small numerical factor of advective instability. The argument for shear instability can be increased by considering a spectrum of internal waves where the lower frequency modes impose an ambient shear environment for the higher modes that enhances breaking conditions. Taking into account a spectrum of internal waves, it is suggested that instabilities can occur due either to advection or shear, depending on wave slope and the ambient shear.

The wave number spectrum of horizontal temperature variations can be divided into several ranges characterized by spectral slope power laws. Garrett and Munk (1972, 1975, 1979) proposed evolving semi-empirical spectral models that have provided impetus for other investigators to acquire data to compare with the models. The Garrett and Munk theory predicts a -2 power law decay at lower frequencies and a -2.5 law at higher frequencies. The internal wave contribution cuts off at the local Väisälä frequency,  $N$ . Above  $N$ , Levine and Irish (1981) have shown a continuation of the -2.5 slope attributed to finestructure alone. At larger wave numbers, buoyancy and convective ranges are found with -3 and -5/3 power laws respectively.

Kolmogorov (1941) theorized that energy was extracted from an unstable mean flow by the largest eddies in a turbulent flow. The turbulent flow, consisting of eddies of various sizes, progressively transferred the energy to the smaller eddies where heat was ultimately dissipated by action of viscosity in the smallest eddies. From this theory,

Kolmogorov predicted a  $2/3$  power law dependence for the structure function for turbulent flow. The transformation of this result to wave number space energy spectra yields a wave number to the  $-5/3$  power law dependence. This was first demonstrated by Batchelor (1953) and later verified by Grant et al. (1962) in the ocean at high wave numbers.

In recent years, there has been a veritable explosion in the number of fine-scale temperature measurements due to the advent of improved instrumentation. Most of the measurements use profiling devices and are concerned with vertical scales. Federov (1978) gives a good summary up to 1974, including much of the Russian literature. More recent reviews and references include Phillips (1977), Turner (1981), Munk (1981), Gargett and Osborn (1981). Greatest attention has been given to comparing the temperature variability about the mean profile and comparing the results with the Garrett-Munk spectra. Due to stationarity constraint, the upper ocean is usually not included in the spectral calculations.

Horizontal microstructure scales in the upper ocean have been measured by thermistors mounted on submarines and towed fish. As early as 1948, Urich and Searfoss utilized a submarine to measure microstructure off the Florida coast at depths up to 50m, and they measured length scales of 20 to 100cm and typical temperature variations of 0.02 to 0.1°C. Leiberman (1951) made similar measurements off Southern California in the depth range of 30 to 60m and calculated

mean patch size on the order of 60cm and an average temperature variation of  $0.05^{\circ}\text{C}$ . Zenk and Katz (1975) used a towed thermistor at 26m depth in the Sargosso Sea. They point out that the use of spectral analysis in a high-frequency range may be seriously affected by the nonstationarity of the horizontal temperature data series due to the patchiness of the temperature variations encountered. Zenk and Katz (1975) calculated 37 sequential spectra, each spectrum representing approximately 1Km. They found the spectral density varied by greater than 30 fold, which is consistent with earlier Russian work reported in Zenk and Katz (1975). More recently, Gibson (1980) measured both temperature and velocity variations with a towed fish. He, and also, Crawford and Osborn (1980) using a free-fall profiler measuring both temperature and shear velocity, found most often that small scale temperature inversions and velocity microstructure occur together. Less frequently, Gibson (1980) found patches of temperature microstructure without velocity microstructure. These patches appear to be the remains of internal waves that had previously broken and are referred to as "fossil turbulence".

Munk (1981) writes, "the picture that emerges is one of a finestructure that is dominated by internal wave straining and is fairly uniform, in contrast to microstructure that is extremely patchy and variable even in the mean."

## B. ACOUSTIC PROPAGATION

To describe wave propagation through the ocean, the basic Helmholtz wave equation for homogeneous media must be modified

to account for changes of the refractive index with space and time. Historically, much of the research into wave propagation through fluctuating media has been derived from theoretical studies of electromagnetic wave propagation in the atmosphere. Treatments based on work by Rytov (1937), Chernov (1960) and Mintzer (1953) have included refractive index fluctuations into the Helmholtz wave equation under different assumptions of isotropy, scale-size, and the strength of inhomogeneities within the media. The methods and predictions of acoustic amplitude variations from this early work are described below, together with a summary of recent extensions of propagation theory including de Wolf (1975) and Flatte (1978).

Mintzer (1953) applied the Born approximation to the basic wave equation. The Born approximation is a perturbation technique which is valid only if the acoustic amplitude fluctuations remain small, and accounts for scattering only from a single turbulent blob within the acoustic path length. The solution yields an expression relating the form of the structure function of the scattering medium to the coefficient of variation of acoustic pulse amplitude,  $V$ . An assumption used in the following three treatments is that during the travel time of an acoustic pulse, the medium remains constant (i.e., the microstructure mozaic remains fixed) and changes in the microstructure occur only between successive pulses.

The following equations and conditions were presented by Stone and Mintzer (1962, 1965) after they conducted a series

of laboratory experiments to check predictions of the variance of normalized sound pressure level in a low frequency (wave equation vs. ray theory) region:

$$V^2 = \frac{1}{2} \sqrt{\pi} K_0^2 \alpha^2 a L \quad (\text{Gaussian } R_x(\rho)) \quad (5)$$

$$V^2 = \alpha^2 K_0^2 a L \quad (\text{Exponential } R_x(\rho)) \quad (6)$$

where

$$V^2 = E\left[\left(\frac{\Delta p}{p_0}\right)^2\right] \quad (7)$$

$p$  = Acoustic pressure

$p_0$  = mean acoustic pressure

$a$  = Taylor structure length scale

= 1.14 × Integral length scale (for Gaussian correlation function)

$L$  = Acoustic path length

$\alpha^2$  = Variance of index of refraction

$\lambda$  = Acoustic wavelength

$$K_0 = 2\pi/\lambda \quad (8)$$

and

$$\lambda \ll 2\pi a \quad (9)$$

$$\lambda \ll 2\pi L \quad (10)$$

The wave region applies when

$$\lambda \gg 2a^2/L \quad (11)$$

Mintzer applied Liebermann's (1951) experimental values to his results and also obtained good agreement between the theoretical results and ocean measurements obtained by Sheehy (1950). The severe wavelength restrictions required by this theory limited its general use.

Chernov (1960) developed formulae relating acoustic amplitude fluctuations to path length and microstructure scale lengths for both ray theory and wave theory regimes. The ray theory, or geometrical optics approach, is a linearization of the wave equation, and employs the assumptions that the scale of the inhomogeneities is large compared to the acoustic wavelength,  $\lambda \ll \lambda_0^2/L$ , where  $\lambda_0$  is the inner scale of the turbulence and transit time is small compared to the rate of change in the refractive index field. This approach ignores diffractive effects and only considers Rayleigh scattering and refractive effects. Liebermann (1951), applying this theory, predicted variations in sound amplitude with the following equations:

$$V_I^2 = \frac{8}{15} \sqrt{\pi} \alpha^2 (L/a)^3 \quad (12)$$

where

$$v_I^2 = E\left[\left(\frac{\Delta p}{p}\right)^2\right] \quad (13)$$

and

$$\alpha^2 = E\left[\left(\frac{\Delta c}{c}\right)^2\right] \quad (14)$$

Amplitude variations measured by Liebermann were larger than those predicted due to temperature inhomogeneities. Liebermann suggested that additional contributions to the fluctuations could be due to biological scattering, chemical relaxation and bubbles in the near-surface region. Upper ocean acoustic measurements made by Sagar (1955, 1957, 1960) showed that sea state was also a contributing element to amplitude fluctuations.

In the wave theory regime, the method of small perturbations developed by Chernov requires that the amplitude of the scattered waves is small compared to the amplitude of the initial wave, thereby limiting the range in which this method can be applied. Since large amplitude and phase fluctuations are often observed in situations where wave theory is still applicable, an alternate method (Rytov) was employed by Chernov to remove the range restriction.

Rytov's method of smooth perturbations was used by Tatarski (1961) to investigate fluctuations of electromagnetic and acoustic waves by developing a stochastic wave model for the atmosphere. It includes the geometrical optics and Born

approximation method as special cases. The restrictions of the model are that the scale of turbulence,  $\ell$ , is much larger than the acoustic wavelength and that the medium is weakly inhomogeneous and quasi-stationary.

The Debye approximation to the wave equation is a general model which describes the turbulent ocean effects on sound transmission without special long range or high-frequency restrictions (Neubert 1970). It contains Rytov's method as part of its solution and reduces to the Born (single scattering) model for

$$\lambda \gg 2 \pi \alpha \sqrt{aL} \quad (15)$$

It predicts a variance

$$V^2 \approx 2 \alpha^2 K_0^2 \ell L \quad (16)$$

where  $\ell$  is the turbulent integral scale.

Much of the recent work in acoustic propagation in the ocean has concentrated on long range propagation experiments, in which the use of acoustics to remotely probe the ocean has been investigated. This research prompted the development of a more unified treatment of both weak and strong scattering regimes. The different scattering regimes for acoustic transmission in the ocean have been mapped into a strength/diffraction parameter space by de Wolf (1975) and Flatte (1979).

The boundaries within which the different propagation theories apply may be defined in terms of strength and size parameters which characterize the inhomogeneities in the ocean. For the isotropic case, Flatte (1979, p. 91) has defined the dimensionless size parameter  $\Lambda$  as

$$\Lambda = L^{-1} \int_0^L (2\pi)^{-1} [R_f^2(x)/L^2] dx \quad (17)$$

Evaluating the integral

$$\Lambda = L/(6 \ell^2 K_0) \quad (18)$$

where  $R_f(x)$  is the radius of the first Fresnel zone for a source and receiver separated by a range  $L$ , and  $\ell$  is the correlation length of the temperature fluctuations and  $x$  is the range from the source.

The ensemble average integral of the sound speed along a straight line between the source and receiver is used to characterize the strength:

$$\phi^2 = \langle (K_0 \int_0^L \mu dx)^2 \rangle \quad (19)$$

where

- $\phi$  = the strength parameter (dimensionless)
- $K_0$  = the acoustic wavelength
- $\mu$  = the fractional sound-speed deviation from the mean sound channel value

For the case where  $R_f \gg \lambda$ ,  $\phi$  can be approximately evaluated as

$$\phi^2 \approx q_0^2 \langle \mu^2 \rangle L \ell_p \quad (20)$$

where  $\ell_p \approx 0.4$  is the integral scale length. Under the geometrical optics approximation the quantity  $\phi^2$  is the rms variation in phase of a pulse at the receiver.

Several important regime boundaries are shown in the representation of  $\Lambda$ - $\phi$  space shown in Fig. 1 (after Flatte 1979, where a full discussion may be found). The geometrical optics and Rytov extension regions have been discussed earlier. The most important boundary in the diffraction region ( $\Lambda > 1$ ) is the line  $\phi = 1$ , where the rms phase fluctuations and the intensity fluctuations both approach unity. Here phase fluctuations are normalized by the acoustic wave period (50 $\mu$ s for 20KHz), and acoustic intensity is normalized by its mean value.

The measurements made in the AVEX experiment will be discussed in terms of their position in this parameter space.

### C. ACOUSTIC PROPAGATION EXPERIMENTS

During the 1950's several ocean measurements of acoustic amplitude were made from drifting ships; see for example Sheehy (1950), Liebermann (1951) and Sagar (1955 and 1957). These authors found amplitude fluctuations significantly larger than their theoretical predictions and suggested that this was due to environmental effects other than temperature

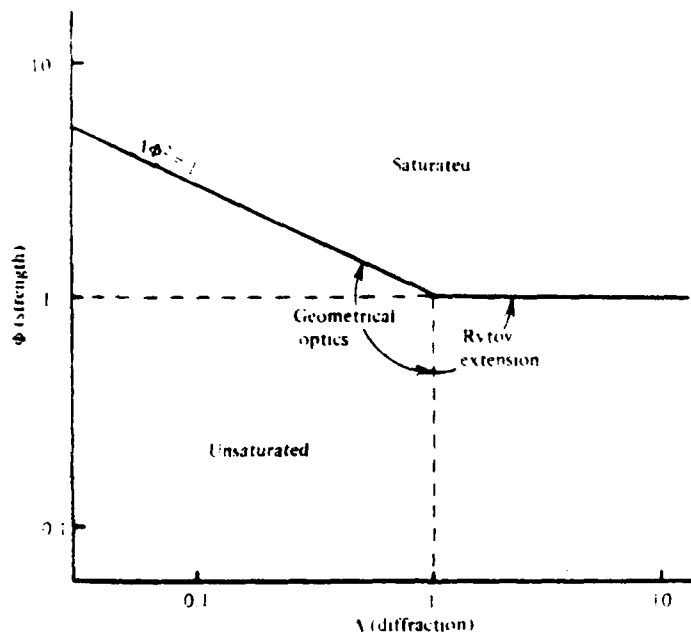


Figure 1. Regimes of  $\lambda$ - $\phi$  space.

inhomogeneities, for example bioscatterers and air bubbles, and measurement problems such as rotation of non-omnidirectional transducers and interference from surface and bottom reflected pulse arrivals. The use of drifting platforms did, however, allow estimates of range dependence to be made relatively easily.

Examples of recent long range acoustic experiments include the MIMI project (see for example Steinberg, et al. (1972) and Clark and Weinberg (1973)) during which 406 Hz pulses were transmitted over a 1250Km wholly refracted path. This long range placed the experiment within the saturated area of Flatte's parameter space; i.e., there were several rays or micro-multipaths from the source to the receiver.

Porter and Spindel (1977) report on a propagation experiment using a ship suspended source and free drifting receiver buoys. An acoustic doppler navigation system was used to measure buoy motion. They calculated frequency spectra of acoustic phase for hydrophones at depths between 300 and 1500m and found that the shallowest receivers exhibited an order of magnitude greater phase fluctuations than predicted by a random multipath model based on sound interaction with internal waves.

Kennedy (1969) measured arrival times and amplitudes of 10ms, 800Hz pulses transmitted over a 25-mile, wholly refracted path. Fixed sources were utilized with an acoustic array of 11 vertically spaced hydrophones with a maximum

separation of 300 feet. Wherever possible, the measured results were compared with the theoretical values of Chernov (1960). Results calculated for phase and amplitude fluctuations compared favorably. Kennedy found evidence that some of the amplitude fluctuations were caused by the interference of secondary scattered waves with the primary wave. Calculations were made using the theory of an inhomogeneous medium with multiple patch sizes as described by Kolmogorov (1941).

Ewart (1976) measured amplitude and phase fluctuations in pulses sent over a wholly refracted path over a range 17.2Km and depth of 1000 meters. Eight-cycle pulses at 4,166Hz and 16-cycle pulses at 8,333Hz were sent alternately every 15.7 seconds and received by three horizontally spaced hydrophones. Power spectra of amplitude and phase fluctuations at single receivers and phase differences for the series of three receiver hydrophones were calculated and compared with theoretical calculations. The amplitude fluctuation spectra displayed strong diurnal and semidiurnal peaks, while the phase fluctuation spectra displayed a third peak at the quarter diurnal frequency. In the spectral band between the inertial frequency for the local area and the Väisälä frequency at 1000 meters, Ewart found power law dependencies with frequency,  $\omega$ , of  $\omega^{-3}$ ,  $\omega^{-1}$ , and  $\omega^{-1/2}$  for phase, amplitude and phase difference spectra, respectively.

In a subsequent analysis of Ewarts data, Desaubies (1976) attributed the source of phase fluctuations with frequencies between the inertial and buoyancy frequencies to be caused

by internal wave activity. He was able to use the geometric approximation in this model, and emphasized that the model was very sensitive to oceanic measurements.

The contribution of fine to micro-scale temperature activity to acoustic amplitude and phase fluctuations was not well defined by the experiments described above. Desaubies (1976) did point out that phase fluctuations are dominated by larger scale sound-velocity variations, whereas the amplitude fluctuations are related to smaller scales. He postulated that the amplitude variations are not caused directly by the internal wave field, but by small scale multipaths caused by the temperature finestructure being advected by the internal-wave field.

### III. ACOUSTIC VARIABILITY EXPERIMENT (AVEX)

#### A. EXPERIMENT DESCRIPTION

Acoustic and oceanic data were acquired from August 2 to August 26, 1979 in the Carmel Canyon of Carmel Bay. Figure 2 is a schematic cross-section of the experiment, and Figure 3 shows a plan view. The bathymetry along the acoustic path had relatively level terrain at depths between 30 and 35m each side of the Canyon and steep slopes to the bottom depth of 180m. A fathometer trace of the bottom profile from the transmitter station to hydrophone station 400m away is shown in Figure 4. The location was chosen because the bathymetry offered the opportunity to have a bottom-mounted, transmitter-transducer and receiver hydrophones located on each side of the Canyon, with no surface or bottom reflected multipath arrivals for the duration of the signal pulse. The use of the rigid, bottom-mounted transducer and hydrophones precluded any biasing of the amplitude and phase fluctuations due to motion of the transducer or hydrophones. The experiment can be segmented into five sites: 1) Station T (Transmitter); 2) Station R (Receiver); 3) Station P (Profiler); 4) Current Meter Array; and 5) Shore Station. The five stations are described separately.

##### 1. Station T

The transmitter tower is shown schematically in Figure 5, and Figure 6 is a photograph of the deployment of the

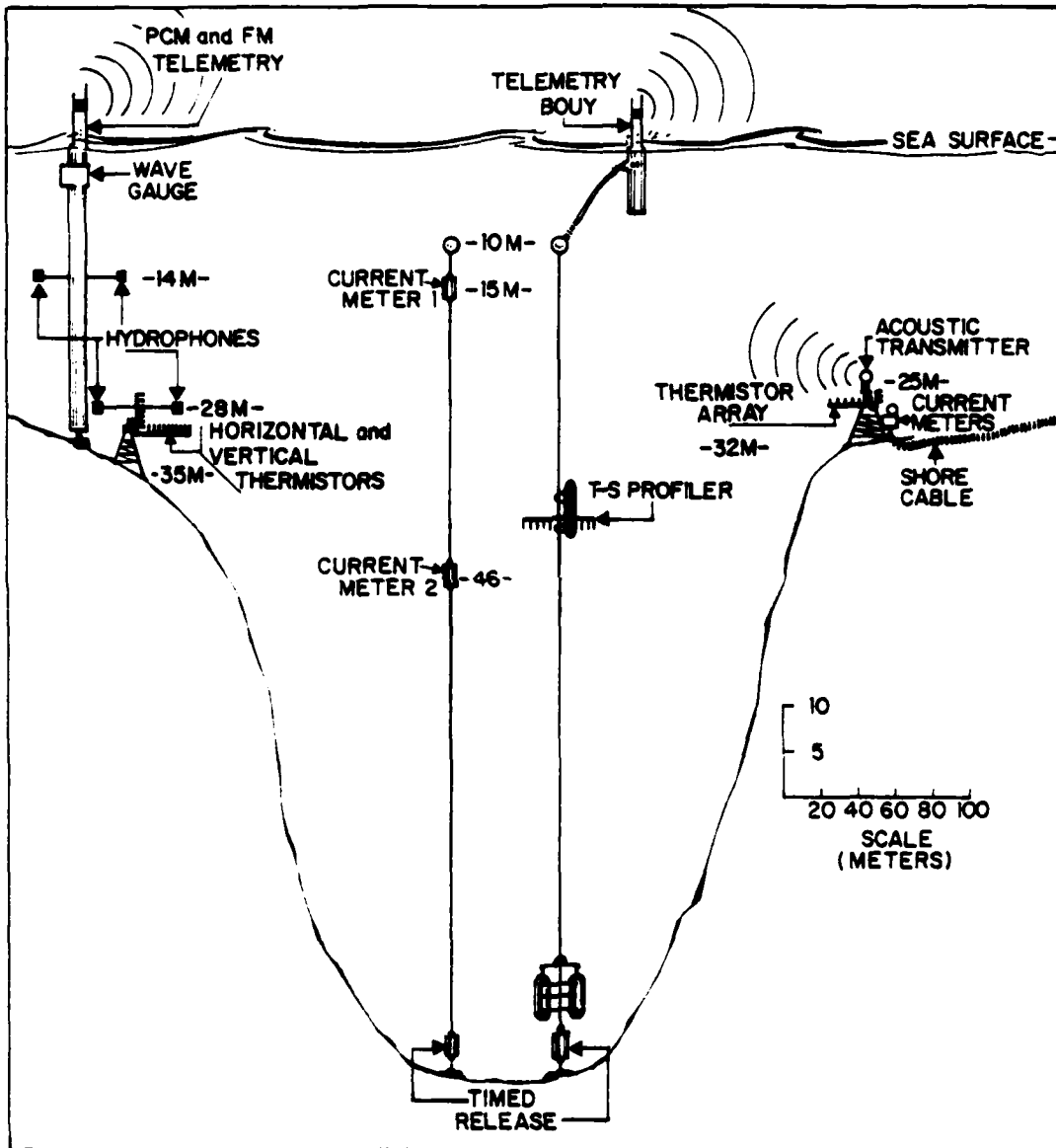


Figure 2. Schematic cross-section of experiment location.

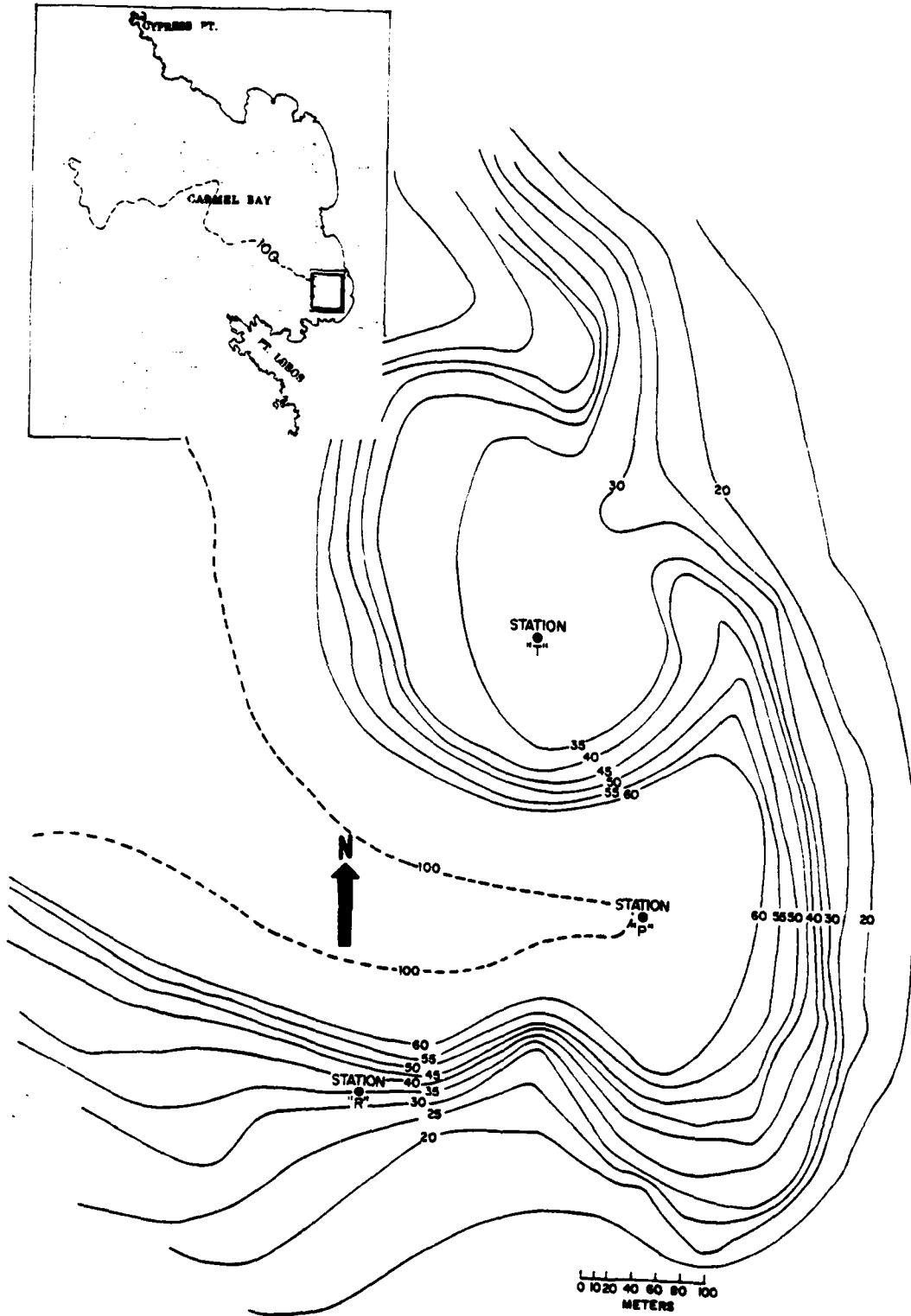


Figure 3. Plan view of experiment layout.

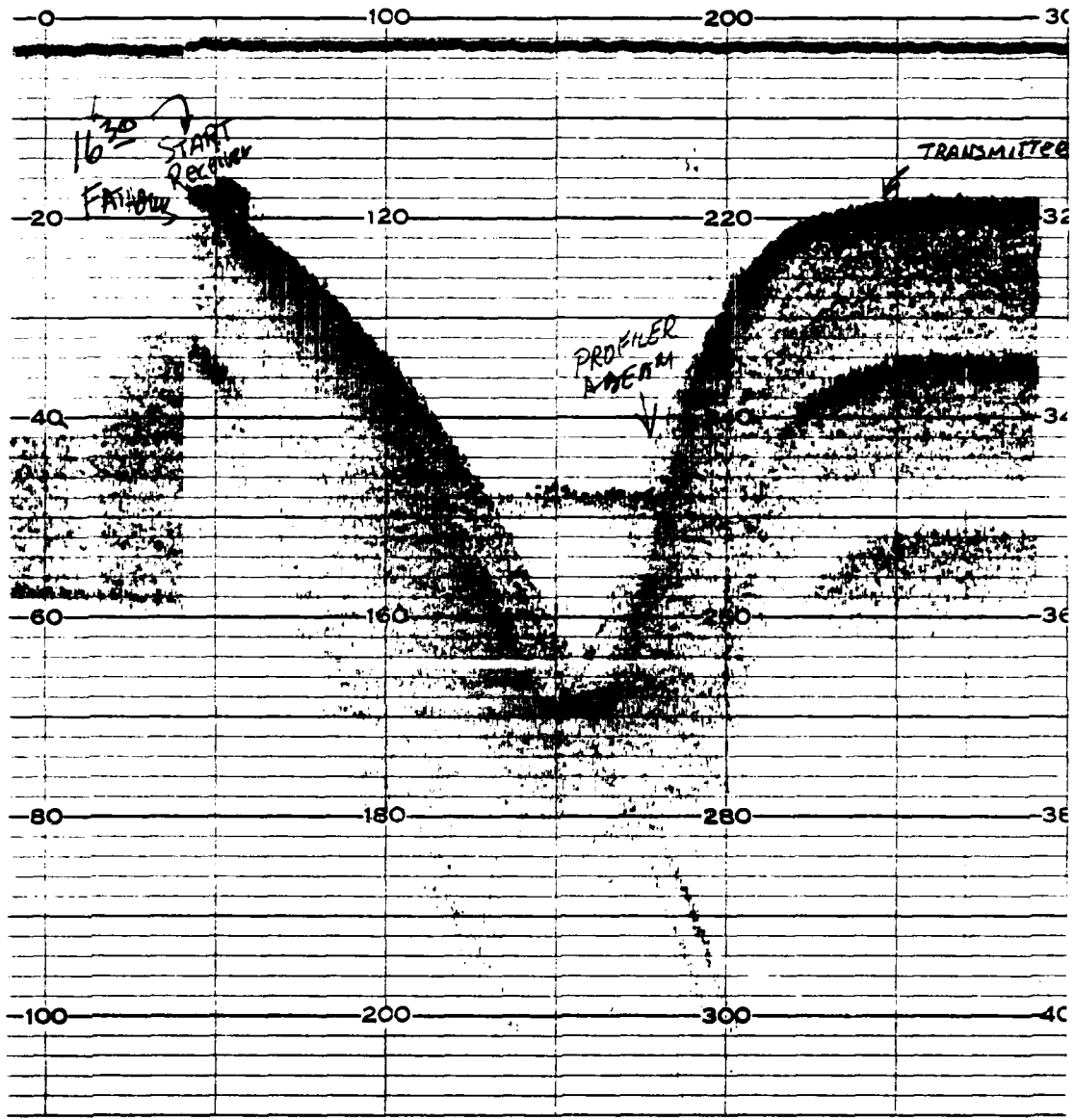


Figure 4. Fathometer trace across Carmel Canyon.  
Depth in fathoms.

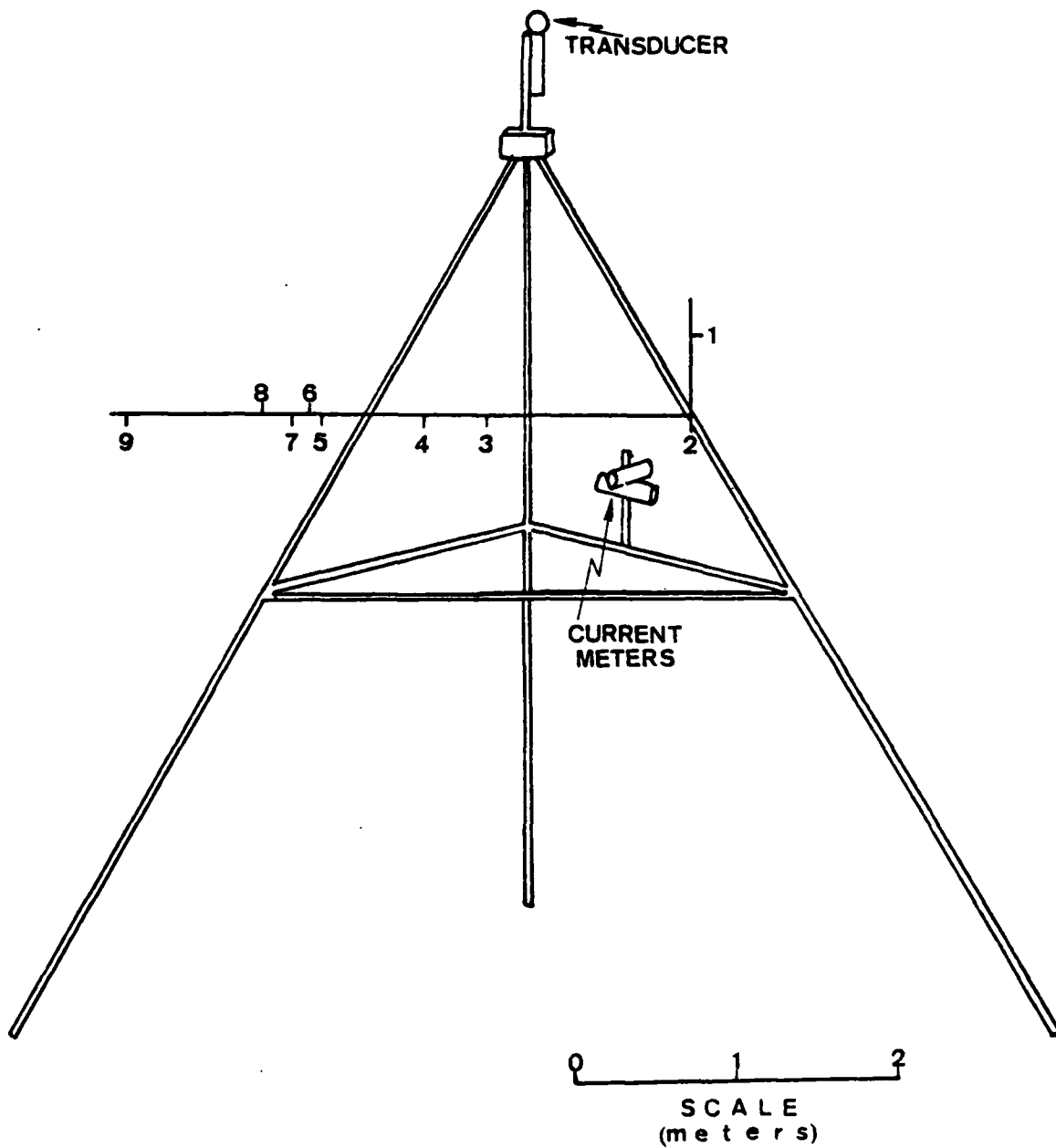


Figure 5. Transmitter tower schematic.



Figure 6. Photograph of transmitter tower.

tower. A spherical, omnidirectional transmitter-transducer was mounted at the top of the rigid tripod, 7m from the base. An omnidirectional transducer was used to ensure the transmission of broad-band signals without the formation of narrow, directional acoustic beams, which would otherwise make the received signal amplitude very susceptible to very small transducer rotations. The tripod was located in 32m of water on relatively level terrain. A thermistor array was attached to the legs of the tripod 4.2m above the bottom. The array consisted of eight horizontal and two vertical thermistors with one thermistor in common. The thermistors were unevenly spaced along the arrays to maximize the number of spatial lags for computing correlation and structure functions. Table I lists the spacings for the three thermistor arrays used in the experiment. Two Bendix current meters were positioned on one cross-member of the tripod to measure orthogonal components of the current. A 100 psig pressure transducer was also mounted on the tripod to measure tide and long period wave formation. The oceanic signals measured at Station T were PCM (Pulse Code Modulation) encoded and cabled back to shore for recording, using half of the 4-conductor cable which also carried the 1Kw signal pulses to the acoustic transducer.

## 2. Station R

Figure 7 is a schematic view of the Receiver Station tripod, including the thermistor array. Figure 8 is a photograph taken during installation. The receiver tripod was

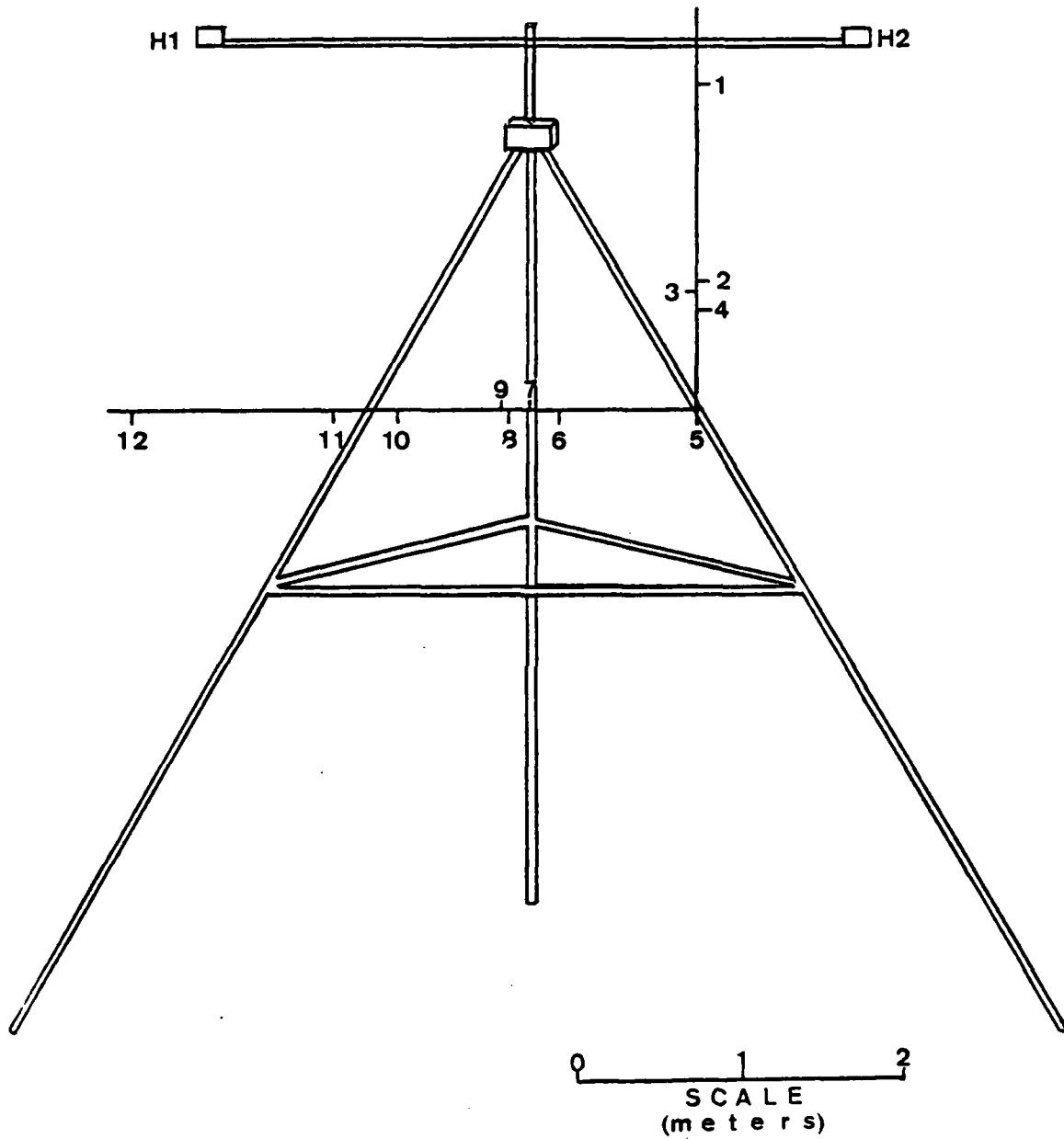


Figure 7. Receiver tower schematic.

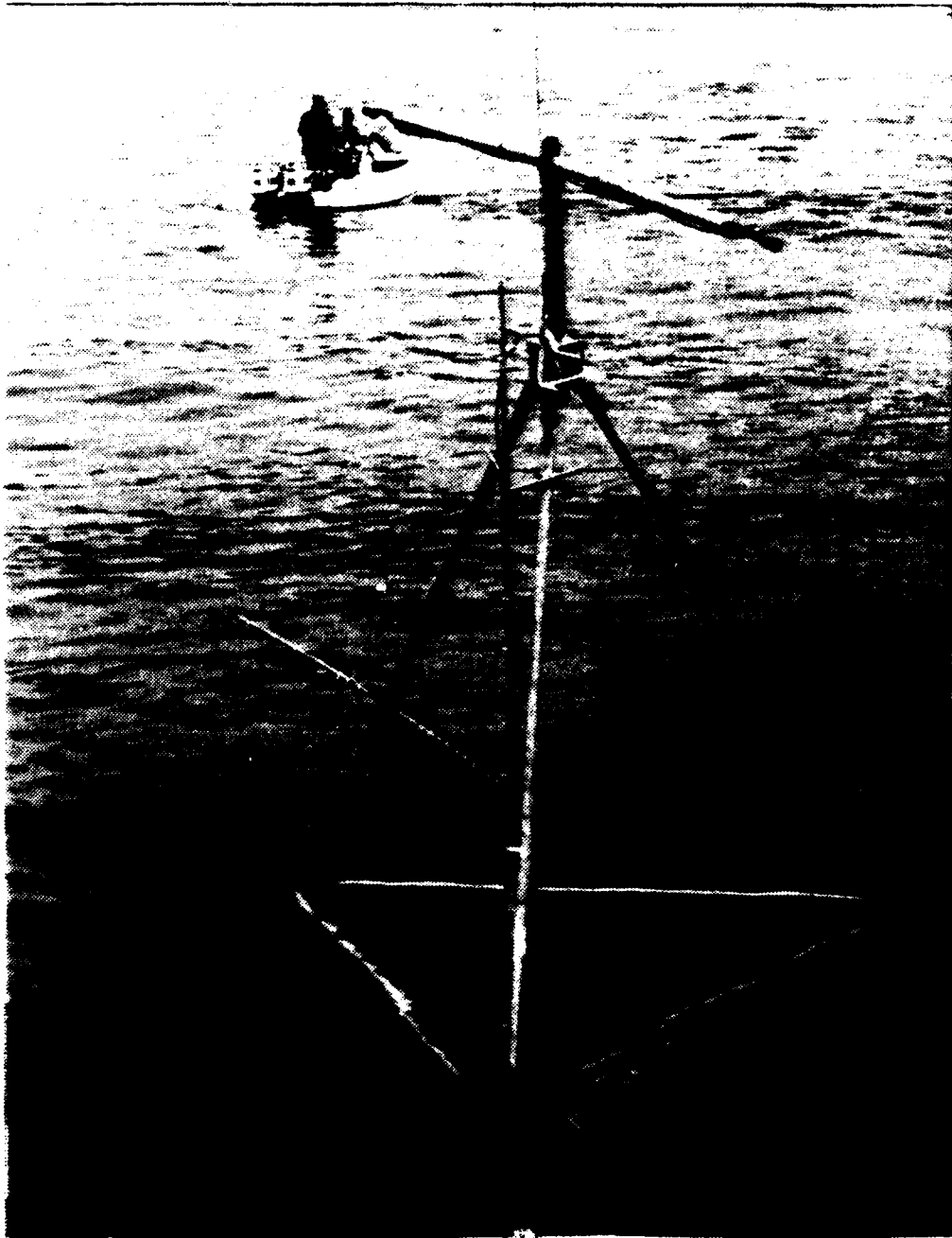


Figure 8. Photograph of receiver tower.

Table I

## Thermistor Array Spacings (cm)

Element	Thermistor Spacings (cm)											
	1	2	3	4	5	6	7	8	9	10	11	12
Station T	48.5	125	40	65	5.5	10.5	20	84.5				
Station R	125.5	5	10	61.5	85	19.5	10.5	5.5	65	40	125.5	
Station P	5	60	50	30	70	10	5	20	35	10	55	

located in 35m of water on a slope of approximately 10 degrees, which required minor adjustments by divers to level the horizontal thermistor array. Eight thermistors were used in the horizontal array, and five in the vertical array, with one common to both. The two-hydrophone array mounted on top of the tripod was 7m above the bottom. The hydrophones were spaced 4.15m apart in the horizontal and oriented approximately perpendicular to the transmission path. Acoustic signals received at the station were VHF, FM telemetered to shore. The measured oceanic data (wave height and temperature) were PCM encoded and also telemetered to the shore.

A 36m vertical spar buoy located 15m south of the tripod supported the PCM telemetry, four-broadband hydrophone telemetry transmitters, two VHF antennas, a two-hydrophone array and a wave gage. The spar buoy was attached to a bottom anchor by a truck universal joint which allowed the spar to free-swivel (but not rotate). The mid-depth, two-hydrophone, horizontal array was located on the spar buoy, 13.7m below the mean water surface with a spacing of 3.86m.

A pressure transducer used to measure waves was positioned just below the lower-low water mark on the spar buoy. The station was powered by a 220 AH 18 VDC, lead-acid battery pack mounted on the tripod.

### 3. Station P

A yo-yo profiler was located near the middle of the Canyon approximately 100m east of the direct acoustic path, as shown schematically in Figure 2. The profiler was designed to make repeated, high-resolution density profiles using a horizontal array of 12 thermistors, a pressure sensor and conductivity cell, by moving up and down a taut-wire mooring cable between the depths of 10 and 100m at approximately 20 cm/sec, once every two hours. Profiling was accomplished by varying the buoyancy by  $\pm 2$  percent of neutral, utilizing a timed variable ballast device. The oceanic signals were PCM encoded, then inductively coupled to the mooring cable. A surface PCM telemetry buoy was tethered from the subsurface profiler buoy and used to VHF telemeter the PCM signal from the mooring cable to the shore station. The yo-yo profiler was damaged during installation and did not function during the experiment. The lack of thermal microstructure at midrange consequently limited the results.

### 4. Current Meter Array

A two-Aanderra current meter array was located approximately 30m south of the profiler, anchored at a depth of 100m (see Figures 1 & 2). The current meters were 15 and 46m below the mean surface, bracketing the sound path. Current

speed and direction data were recorded internally in digital format at 5-minute intervals for the 26-day period. The array was retrieved by the use of timed releases.

#### 5. Shore Station

A mobile bus, serving as the shore station, housed all the receiving, pre-processing and recording equipment. Figure 9 is a photograph of the 10m weather tower attached to the bus. The environmental instruments measured insolation, back-scattered radiation, wind speed and direction, and barometric pressure. Signals were received at the bus via PCM or FM telemetry from Stations P and R, and via the armored cable from Station T.

#### B. INSTRUMENTATION

Table II is a summary of the measurement devices utilized in the experiment and pertinent information on each instrument.

Sound pulses were emitted by an omnidirectional transducer type C7JP3. Omnidirectional hydrophones from AN/SSQ57A sonobuoys were used as receivers.

Temperature was measured using Victory Engineering Corporation .020 inch bead-in-glass probe thermistors. The thermistors had a still water time constant of 55ms and a dissipation constant of 0.75 MW/°C. A Hewlett-Packard HP2801A quartz thermometer with an accuracy of  $\pm .005^{\circ}\text{C}$  was used to calibrate the thermistors through their associated preconditioning electronics and PCM encoder. Calibration was accomplished

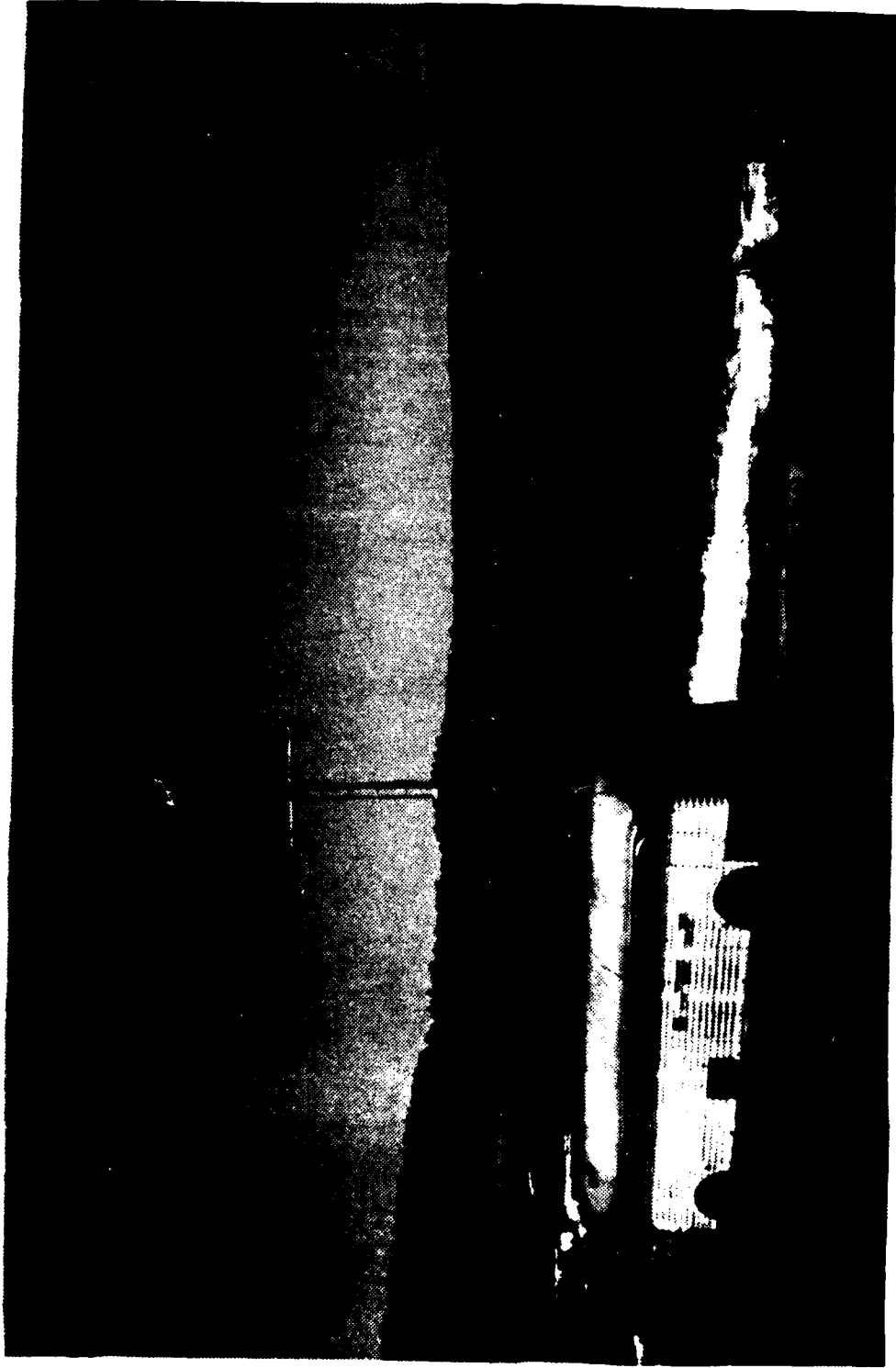


Figure 9. Photograph of shore station.

Table II. Instrument Summary

INSTRUMENT	MANUFACTURER	MODEL	RANGE	ACCURACY	
				LIMITING PARAMETER	RESOLUTION
Thermistor	Victory Engineering Corporation	42A70	6 -16 C	Digitising increment of PCM Encoder	2.5 m°C
Hydrophone (Station R)	Spartan	AN/SSQ-57A	NA	Clipping level of telemetry	-
Current Meter (Station T)	Marine Advisers Inc.	8-10	0-5 KTS	Starting threshold	.04 knots
Current Meter (Canyon)	Aanderaa	RCM4	1.5-250 cm/sec	Starting threshold	1.5 cm/sec
Pressure Transducer (Station T)	Transducers, Inc.	5AP-69F	0-100 psia	Non-linearity & hysteresis	.5 psi
Pressure Transducer (profiler)	Teledyne Taber	2101	0-200 psia	Non-linearity & hysteresis	.1 psi
Conductivity (profiler)	Sea-Bird Electronics	SBE-4	2-5 S/m (see data)	Digitising increment of PCM encoder.	10 <sup>-3</sup> S/m
Pyranometer (shore station)	Eppley Laboratory, Inc.	PSP	0-2800 watts/m	Sensor Accuracy	0.5%
Wind Speed (shore station)	Meteorology Research, Inc.	1022 s	0-35 ms <sup>-1</sup>	Sensor Threshold	.25 ms <sup>-1</sup>
Wind Direction (shore station)	Meteorology Research, Inc.	1022 D	0-540°	Sensor Threshold	4°
Pressure Transducer (spar buoy)	Transducer Inc.	5AP-69F	0-50 psia	Nonlinearity & hysteresis	.15 psi

by cooling a 3 liter volume of water down to 3°C. Thermistors from each array together with the reference quartz thermometer were placed in the stirred volume of water and the system was allowed to slowly warm to 20 °C (ambient temperature). The thermistors were connected to an HP-9845 computer via their preconditioning electronics, PCM encoder, and PCM decoder. The computer recorded and stored measurements every 0.5°C. A least-squares linear fit over the temperature range of 8-16 °C was then calculated for each thermistor.

Currents were measured by both ducted impeller and Savonius current meters. The ducted impeller current meters, mounted on the transmitter tower, were Bendix Corporation, model B-10. The impeller assembly had a starting threshold of 2 cm/s, a threshold of linearity of 3 cm/s, and a response time less than 0.1 second. The impeller rotations were sensed through a magnetic read switch. Flat impeller blades were used for equal responses for both forward and backward flow. Aanderaa meters, model RCM4, were used to measure currents at the mid-Canyon current meter array. These recording meters use a Savonius rotor current velocity sensor and a magnetic compass for direction determination.

Sea surface elevation was measured using a Transducer, Inc., pressure transducer, model 5AP-69F, mounted on the receiver station spar buoy.

Insolation and back-radiation were measured using two, model PSP, Eppley precision pyranometers. Wind speed and direction were measured using a wind speed sensor, model

1022S, and a wind direction sensor, model 1022D, manufactured by Meteorology Research, Inc.

### C. PROCEDURE

Acoustic and oceanic data were collected for 28 min every two hours starting 7 PM August 2 to August 26, 1979. The acoustic pulses were transmitted from Station T transducer, received at the Station R hydrophones, and telemetered to shore where they were processed and recorded. The measurement cycle consisted of the transmission and reception of ten 6 KHz sinusoidal pulses immediately before and after a series of 300 composite pulses, each at a repetition rate of 5 seconds. Complex spectra of three, one-minute average, 4-25 KHz ambient noise spectra received by hydrophones H1 and H2 were recorded at the end of the pulse measurements.

The 6 KHz acoustic pulses were used to assist in the detection of multipathing. The 300 composite pulses were analyzed to obtain phase and amplitude fluctuations of the 20 KHz sine wave and broadband signal contained in each pulse. The 5-second pulse repetition rate was determined principally by the data transfer and processing times, and was long enough for the reflected and reverberated signals of one pulse to decay before the transmission of the next pulse.

An example of the composite pulse is shown in Figure 10. The first 0.6 ms of the pulse consisted of 12 cycles of a 20 KHz, zero phase start and zero phase finish, sinusoidal wave, followed by 4.5 ms of pseudo-random noise. The pseudo-random

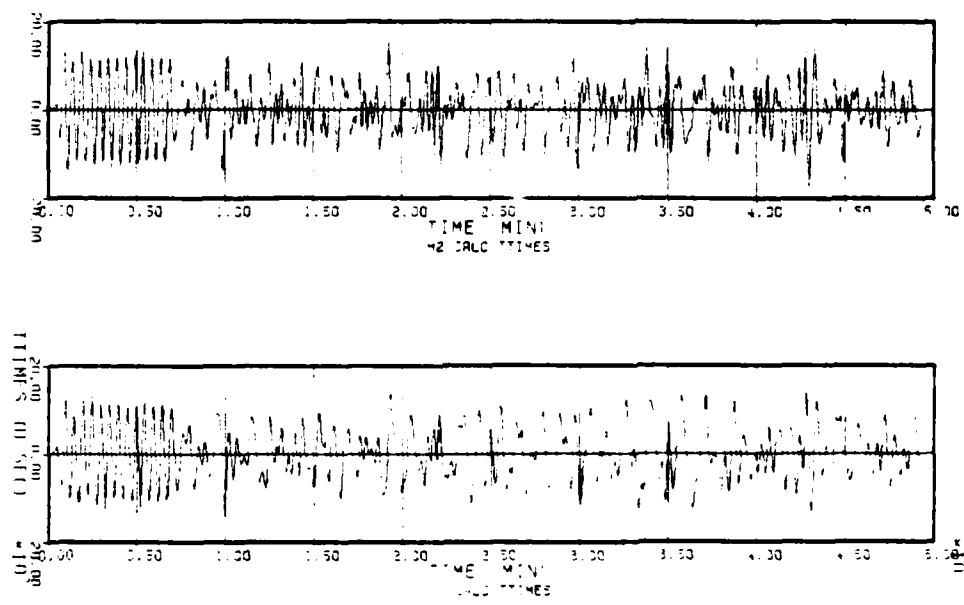


Figure 10. Current wave form of the composite signal pulse (upper panel), and voltage wave form of the composite signal pulse (lower panel).

signal had a flat frequency spectrum from 5 to 25 KHz. The signal was repetitious and identical for each composite pulse. Each time the HP-9845 computer activated the pulse generator, the digitizing delay generator and timer units were initiated. The signal was fed from the pulse generator to a 1 Kw, 300 VRMS power amplifier. The amplifier output provided a 5 to 25 KHz bandwidth constant current source to the transducer via the shore cable. The high powered amplifier was required because of the need to use an omnidirectional transducer while maintaining an acceptable signal to noise ratio at the receiver hydrophones. Frequencies below the 5-25 KHz pseudo random noise band were filtered out to prevent clipping in the constant-current amplifier. The 1 KW output amplifier was used in a constant current mode to enable the transmitted spectrum to equal the input spectrum, despite the complex impedance characteristic of the cable and transducer.

The acoustic pulses were received by the four hydrophones at Station R. The receiver station was synchronized to the transmitter so that only the 5 ms sound pulse would be recorded. Synchronization was accomplished by establishing the pulse generation times and delaying the recording by the 256 ms required for the pulse to travel the wholly refracted path. The received signals were first fed into underwater preamp units and then telemetered to the shore station via 5 to 25 KHz bandwidth FM transmitters, utilizing modified AN/SSQ-57A sonobuoy components.

The signals were received at the shore station by an ARR-52A four channel sonobuoy receiver. Figure 11 schematically shows the data acquisition and real time processing system located at the shore station. All four hydrophone signals were fed to an analogue sample and hold unit, while H1 and H2 were also fed to the dual-channel spectrum analyzer.

Each channel of the analogue processor had a quasi-integrator, gating unit, threshold detector, and sample and hold system. Amplitude and phase fluctuations of the 20 KHz signal were simultaneously measured by a quasi-integration of the positive half of the signal. The signal was passed to the sample and hold unit once a preset threshold was exceeded, during a computer controlled acquisition time-window. The sample window width was set at 3 ms in order to minimize the effect of ambient noise pretriggering the sample and hold unit, and thereby producing erroneous data. Representative voltages were stored in the sample and hold unit until addressed by the Hewlett-Packard 9845, where, one channel at a time, the signals were measured by a scanner and five digit DVM, and subsequently logged into the data acquisition system. During the same 5-second cycle, the atmospheric data (wind speed and direction and insolation) were also scanned, measured and logged into the computer.

The 5 ms time records for H1 and H2 (the two bottom-mounted hydrophones) were digitized to 12 bit accuracy by the spectrum analyzer after a predetermined digital delay initiated by the pulse generator circuitry. For each pulse,

# DATA ACQUISITION AND REAL-TIME PROCESSING SYSTEM

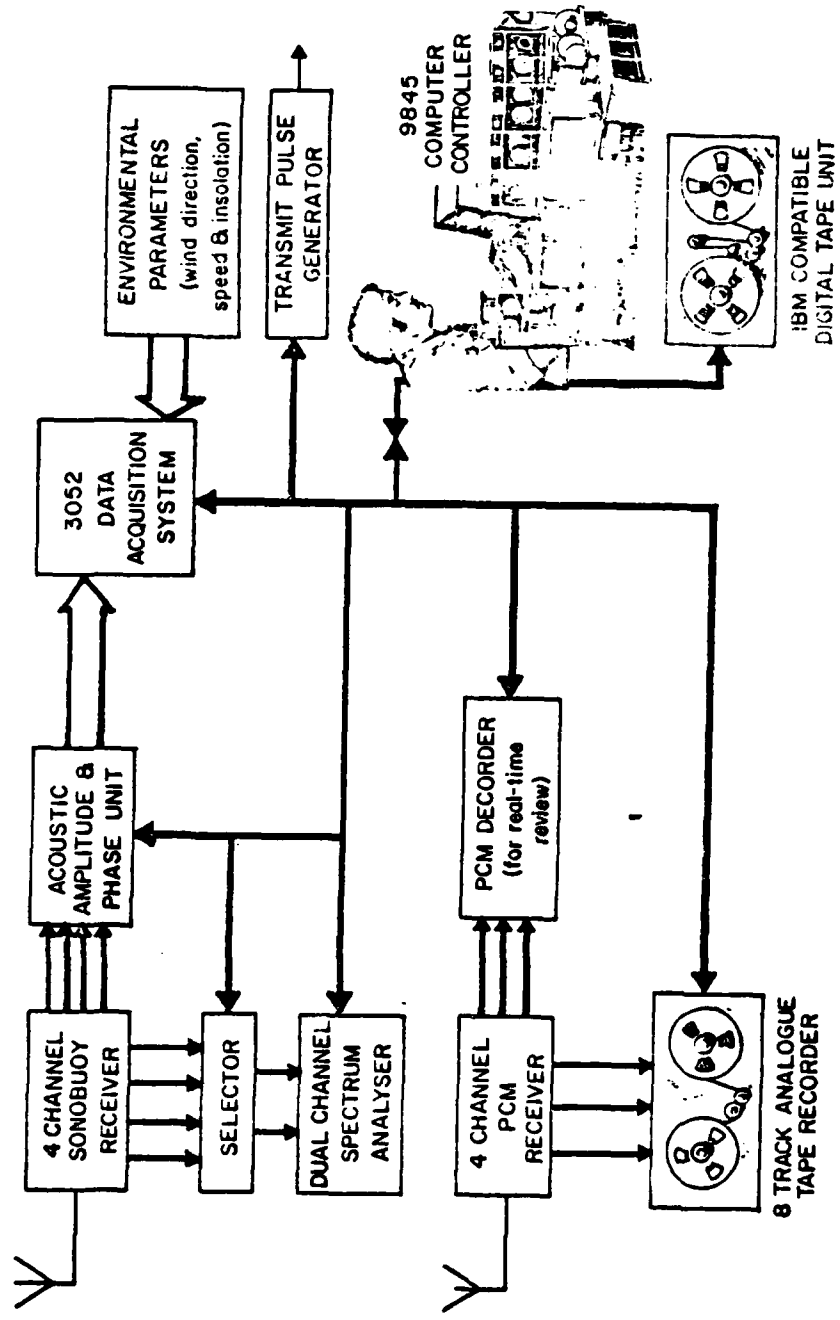


Figure 11. Data acquisition and real time processing schematic

the two 1024 point, 5 ms records were transferred to the Kennedy 9832 digital tape recorder via the computer. The digital delay was set at 256.5 ms (the travel time between transmitter and receiver station) with an accuracy of 100 Nanoseconds.

The schematic diagram of the real time processing and recording of oceanic data is also shown in Figure 11. All oceanic measurements were sampled at a rate of 32 samples per second by the PCM encoders. The remote stations (R & P) were actuated every 2 hrs for 30 min by crystal controlled clocks.

From each of the offshore stations, the analog data was sent to an analog preconditioning unit and then to a PCM encoder, where a serial bi-phase output, including the data and synchronizing words, was telemetered to shore. The signals were received via a four channel PCM receiver system (one channel per station) and recorded on an eight channel analog tape recorder. At the same time, selected channels were sent through a PCM decoder for real-time viewing and analysis on an oscilloscope and chart recorder.

#### D. DATA PROCESSING

The four-day period from 15 through 18 August was chosen for this preliminary analysis. The acoustic data were digitally recorded in a format compatible with the NPS main-frame computer. However, it was discovered that the Kennedy 9832 recorder was faulty during the experiment, resulting

in some lost data and other byte shifted data. The byte shifting problem, although sparse, required complicated additions to the data analysis scheme to check for byte shifts, and make corrections where possible. The oceanic data was pre-processed by the HP-9845 computer to generate IBM compatible data tapes.

#### 1. 20 KHz Acoustics Data Processing

Two methods were used to determine the amplitude of the 20 KHz sinewave pulse transmitted at the start of each composite pulse. The first technique used analog sample and hold processors which measured in real-time the peak value of the positive half of four cycles of the 20 KHz pulse. The second estimate of the 20 KHz amplitude was obtained from computer analysis of the digitized hydrophone signals.

During the first stage of the signal processing, the precise arrival time of the pulse was determined from the cross-correlation between a section of the received pseudo-random noise pulse and a reference transmitted signal. This arrival time was used to identify the beginning and end position of each 20 KHz pulse. The RMS energy of the signal was then calculated over 8 of the 20 KHz cycles and then stored. The time series of acoustic amplitude and travel-time obtained from these two methods were plotted and stored on disk for further analysis.

#### 2. Oceanic Data Processing

A data processing chain under computer control was developed to decode, deglitch and sort the PCM encoded oceanic

data gathered at the shore, transmitter and receiver stations. Data from one station at a time was time synchronized and the serial data stream switched to the PCM decoder. The decoded data were passed to a HP-9845 where the channel identifiers were stripped and the data deglitched according to slew-rate criteria selected for each channel. These data were then averaged to reduce the effective sampling rate from 32 per second to 2.7 per second, and the 4096 data points from each channel were then temporarily stored on digital cassettes. When all three stations had been preprocessed, simple statistics were calculated and printed for 30 selected output channels. The statistical information and the preprocessed data were then transferred to IBM-compatible digital tape.

#### IV. DATA ANALYSIS

Four days, 15-18 August 1979 are described and analyzed for this preliminary examination of AVEX results. The weather during the four days was overcast, with fog in the morning and only very occasional partial clearing (in the afternoon of 16 August). The winds were generally light, with light winds during the night and morning, and increasing to 10 knots or less in the afternoon. The barometric pressure held steady at 30.0 in. of mercury.

The gross temperature profiles were measured with XBT's and reflected the rather constant atmospheric conditions during the four days. The sea surface temperature varied little from 13°C. The profiles showed a very gradual shallow thermocline in the upper 10m, then a partially mixed layer down to about 50m, a thermocline to about 100m and then isothermal conditions to the bottom temperature of about 10°C. The calculated Väisälä frequencies at the 30m depth of the transmitter and receiver, based on the temperature profiles, were high, ranging between 0.05--0.1 hz.

The temperatures, current speed and direction measured by the Aanderra current meter at 46m in mid-Canyon, and tidal elevation for 16 to 18 August are shown in Figure 12. The tidal elevations were measured at Wharf Number Two in Monterey harbor, 10 Km to the north, and there appears to be a slight lag with the current meter data. The current speeds were

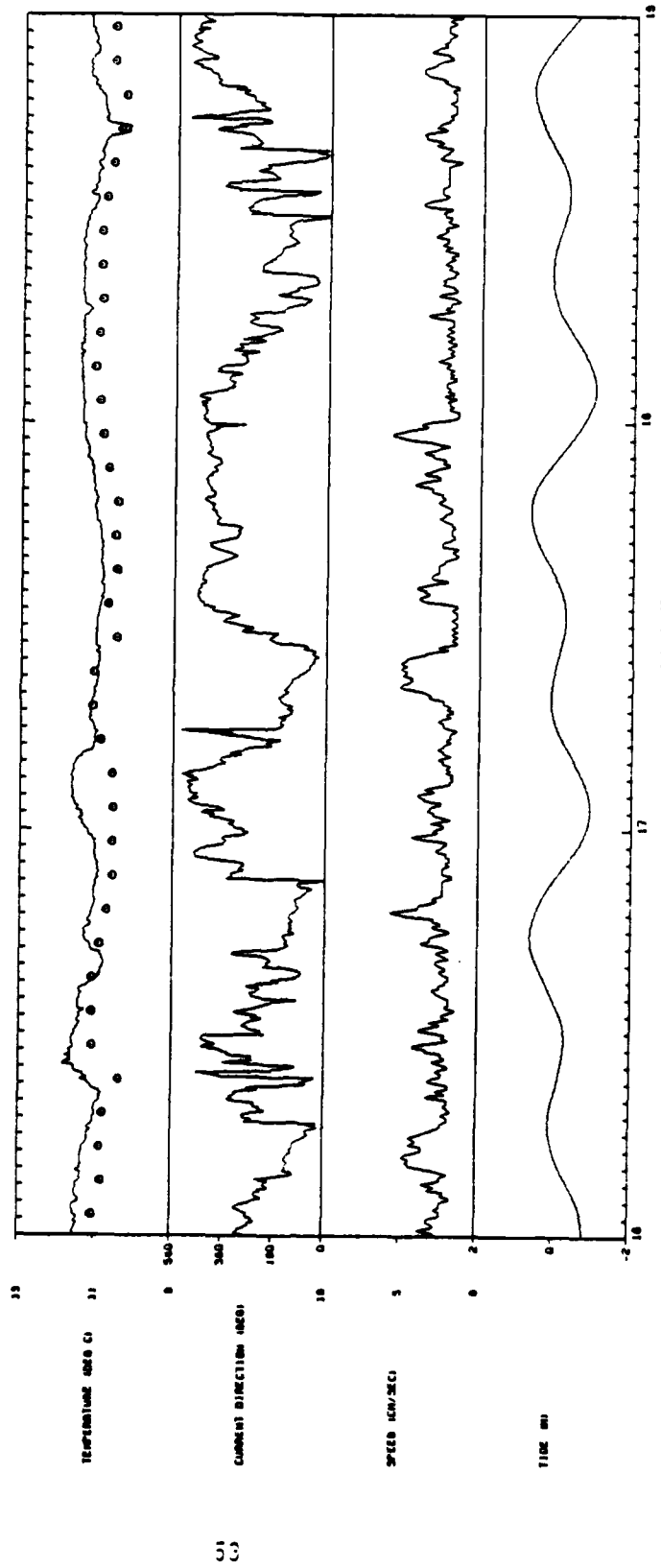


Figure 12. Temperature, current direction and speed, and tidal elevation measured with the 46m depth Aanderra current meter in Carmel Canyon.

generally weak and show a definite tidal component with considerable variability superposed. The current direction signal is noisy and unreliable because the current speeds were near the threshold for the vane. The tidal contribution to the temperature signal is not as obvious, but considerable micro-structure in the temperature signal can be observed.

A log-log, frequency spectrum of the temperature fluctuations for the 18-day period 5-23 August is shown in Figure 13. Identifiable peaks in the spectrum are the inertial period (0.049 cph) and the semidiurnal tide (0.081 cph), and its first and second harmonics (0.161 cph and 0.243 cph). At higher frequencies, the spectral level decreases in the internal wave region. The -2 and -2.5 spectral slopes proposed in the Garrett-Munk (1979) internal wave model are indicated. At the highest frequencies, the spectrum flattens out into the microstructure region. The spectrum appears noisy because it was calculated with only 8 degrees of freedom to resolve the inertial and tidal peaks.

Examples of 25-min oceanic data starting on hours 0100, 0300, 0700, and 0900 on 17 August are shown in Figures 14-17. Starting at the top of each figure, the measured variables listed on the left hand side of the figures included: barometric pressure, back radiation, incident radiation, wind direction, wind speed, receiver tower battery voltage monitor, water surface elevation, thermistors on the receiver tower R12-R1, ducted current meters on transmitter tower CM2-1,

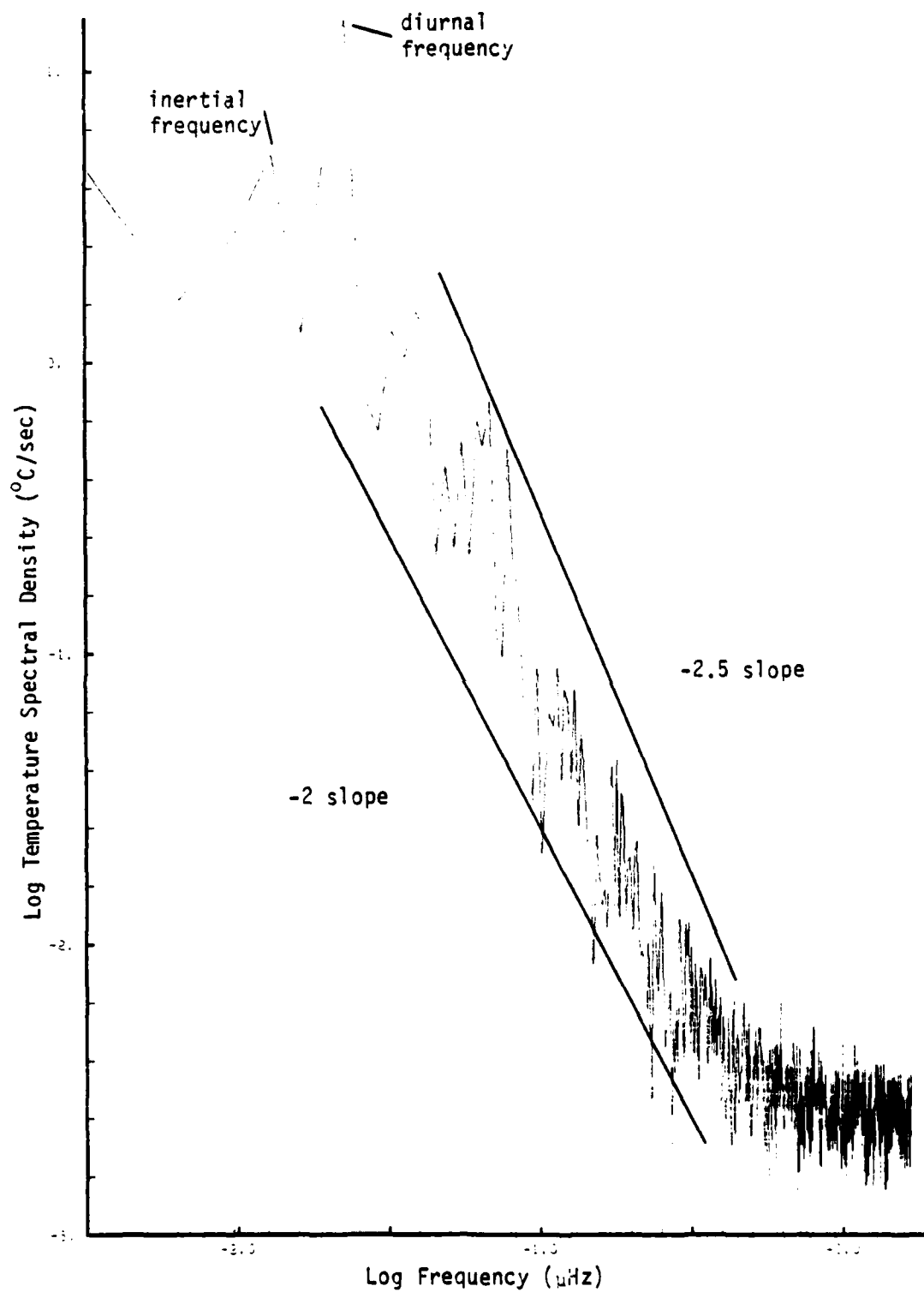


Figure 13. Spectrum of temperature fluctuations at 46m depth in Carmel Canyon, 5-23 August 1979.

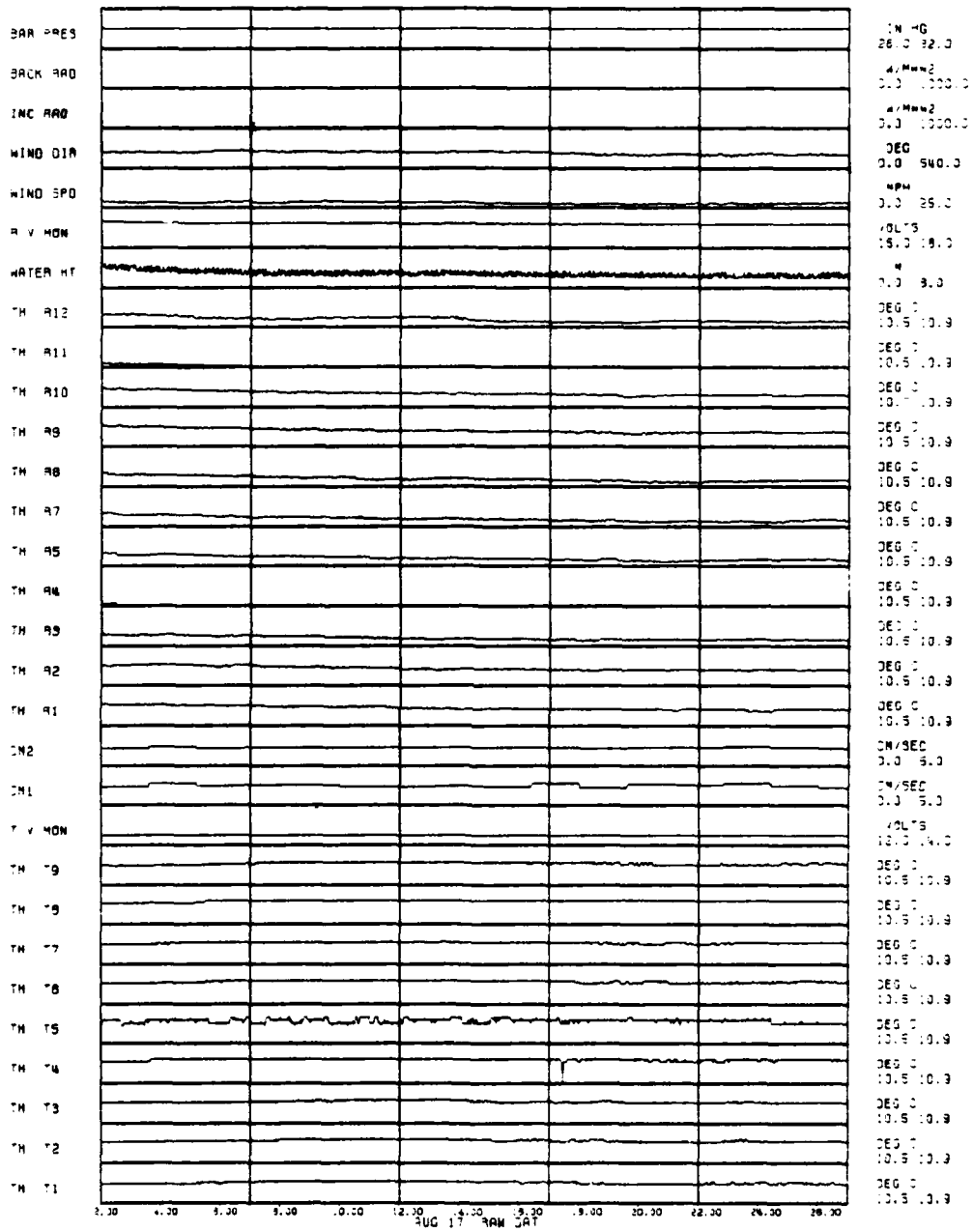


Figure 14. 25-minute environmental data records starting 0100 hours, 17 August.

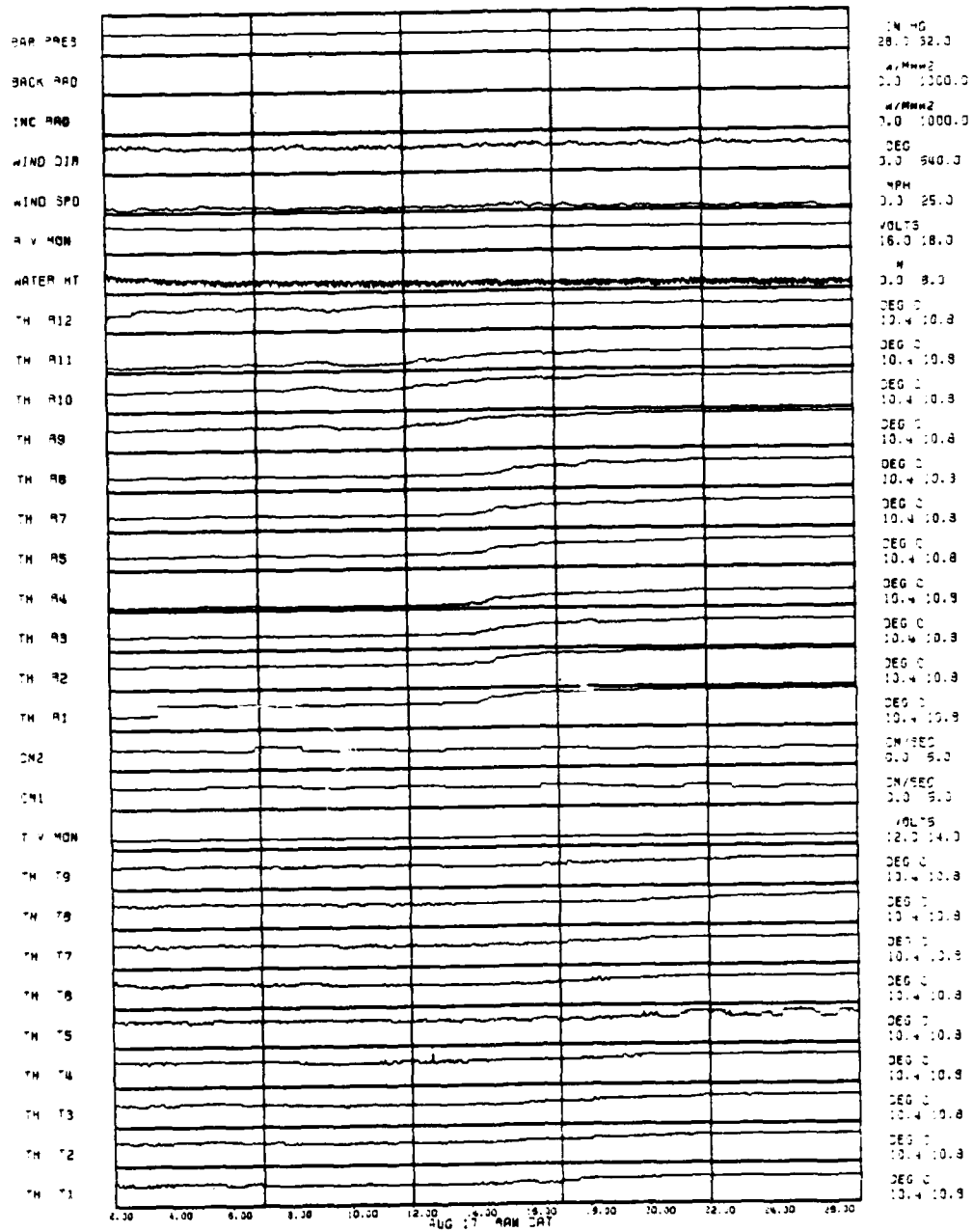


Figure 15. 25-minute environmental data records starting 0300 hours, 17 August.

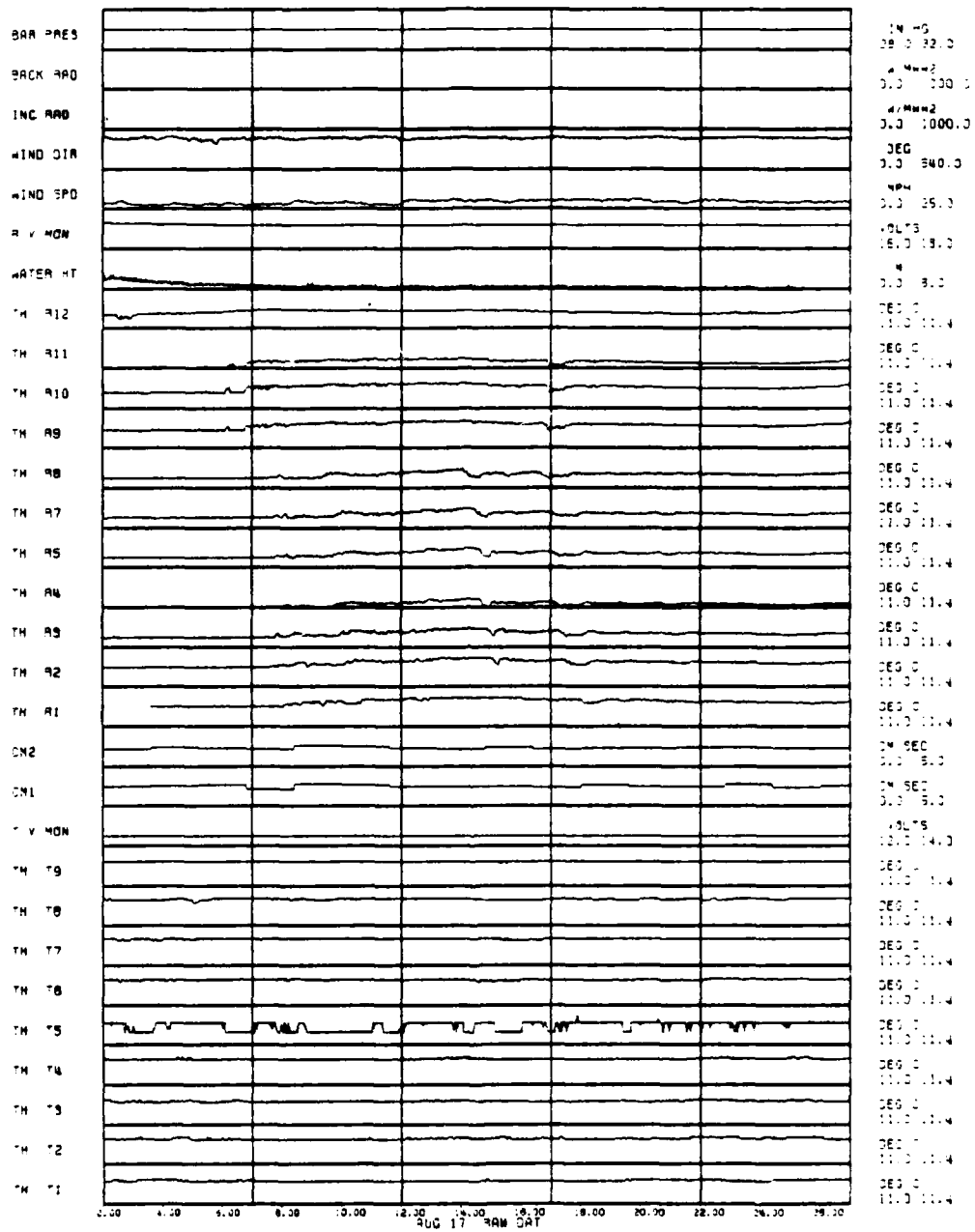
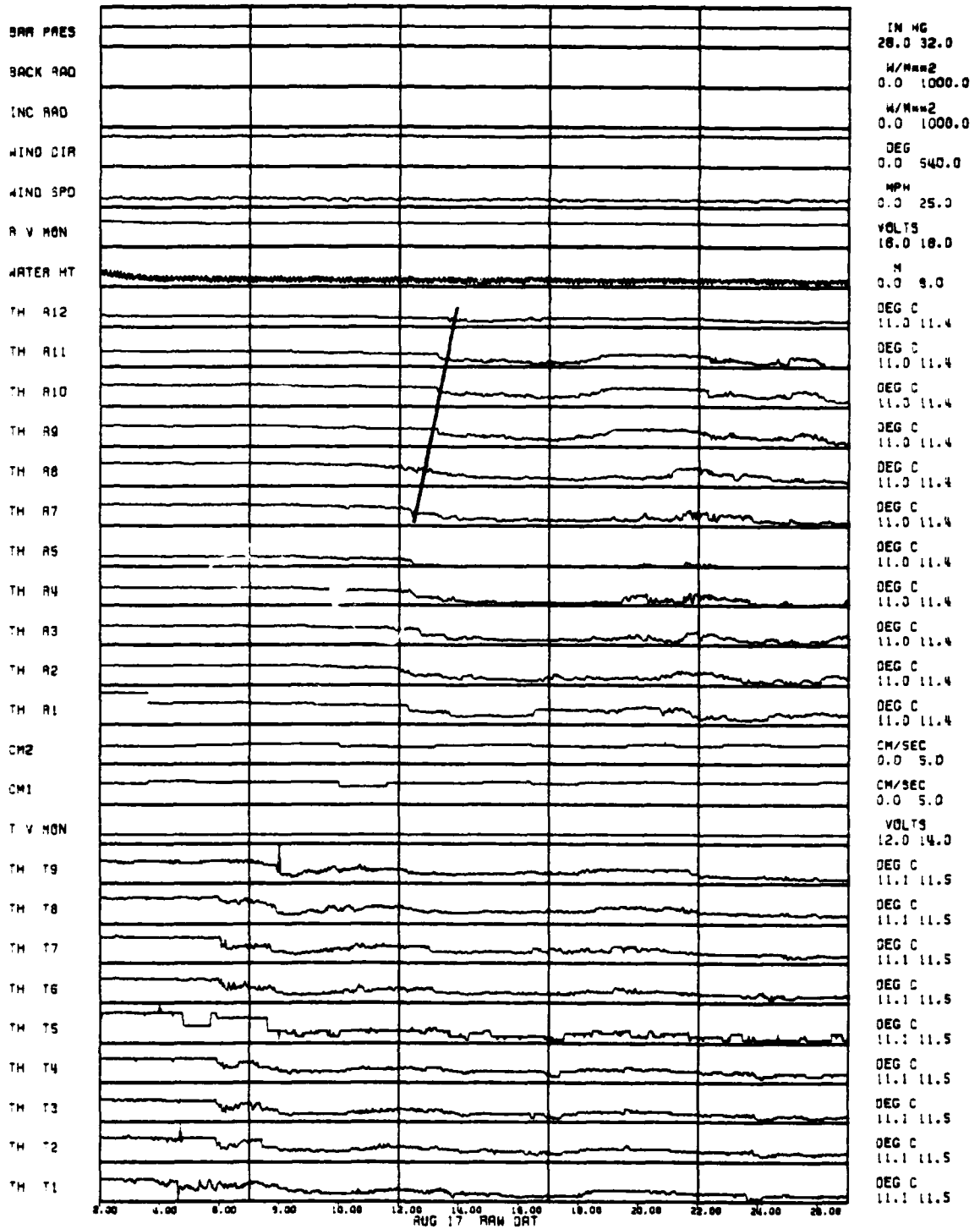


Figure 16. 25-minute environmental data records starting 0700 hours, 17 August.



900.

5.

Figure 17. 25-minute environmental data records starting 0900 hours, 17 August.

transmitter voltage monitor, and thermistors mounted on transmitter tower, T9-T1. The units and range of plot values are listed on the righthand side of figures. Thermistors on the transmitter tower, T9-T1, have glitches due to the feedback of biphase encoded signals into sensitive thermistor signal conditioners, and were not analyzed. All the other sensors shown in the figure worked well. The temperature microstructure time series showed great variability. Focusing attention on the thermistors at the receiver tower in Figures 14 to 17, recall that the vertical array consisted of thermistors R1 to 5 and the horizontal array contained thermistors R5 to 12, with R5 common to both (see Figure 7). At 0100 hour, the mean temperature was relatively constant at 10.5 °C with visible microstructure. During 0300 hour, a portion of an internal wave is visible going from the crest (colder water brought up) to the trough (warmer water) with a change of about 0.2 °C. The waves shapes are very characteristic of nonlinear internal waves propagating onto a shelf (see Phillips, 1977, p. 199).

The time series during 0700 hour appears to show a short period internal wave trough upon which extensive microstructure is observed. An internal wave going from the trough to crest appears during the 0900 hour record with very extensive microstructure and high frequency internal waves occurring. The gross temperature variations appear consistent with internal waves slowly propagating by the array, and less correlated microstructure, that at times is reminiscent

of billow turbulence caused by wave breaking. Propagation velocity can be calculated from the thermistor arrays by observing the travel time of the wavefront across the array. Referring to Figure 17, for example, a line connecting the wavefront across the seven horizontal thermistors indicates a time of about 100 seconds to travel the 340cm, which corresponds to a velocity of 3 to 4 cm/sec; this speed is consistent with the velocities measured in the center of the Canyon with the Aanderra current meter.

Correlation lengths were measured from the calculated autocorrelation functions. Examples of structure functions and autocorrelation functions calculated for the same horizontal and vertical thermistor arrays at the hours 0100, 0300, 0700, and 0900 on 17 August are shown in Figures 18 and 19. The structure functions and autocorrelation functions were calculated using all combinations of thermistors possible. The heavy horizontal bar indicates the length of the arrays. In general, the arrays were too short to completely measure the structure and autocorrelation function, particularly in the horizontal. Integral scale lengths, corresponding to the average eddy size, were calculated from the area under the autocorrelation functions. The integral scale,  $\lambda$ , is defined

$$\lambda = \frac{\int_0^{\infty} R_x(\rho) d\rho}{R_x(0)} \quad (21)$$

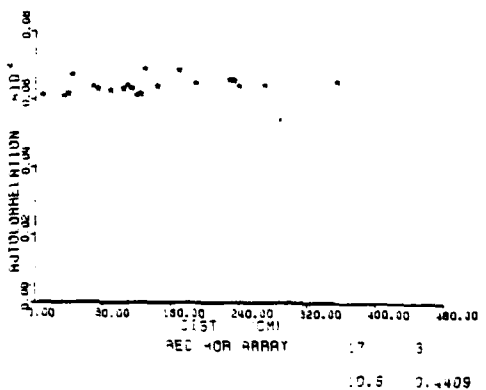
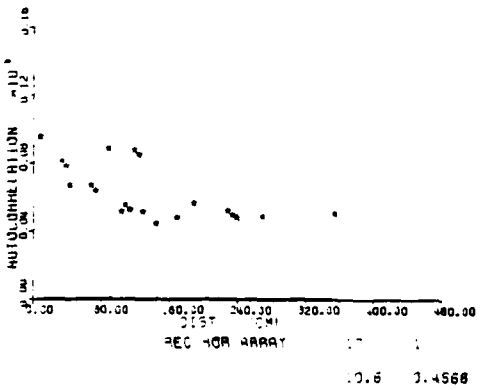
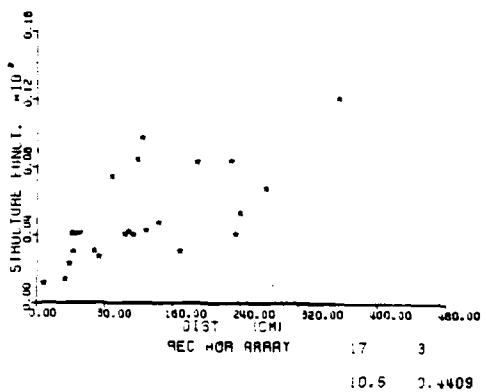
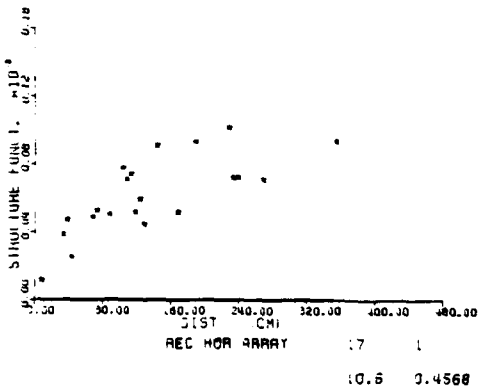
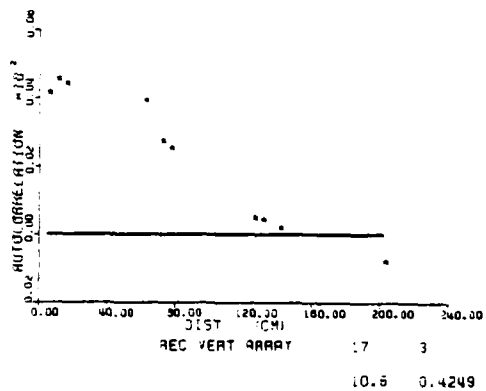
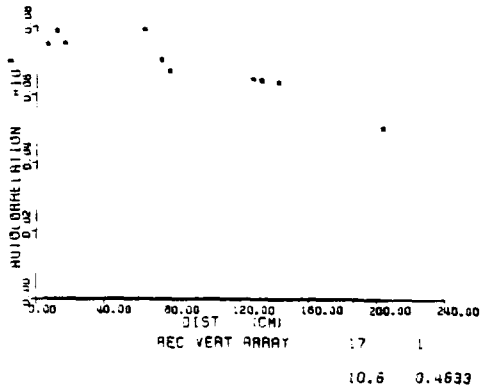
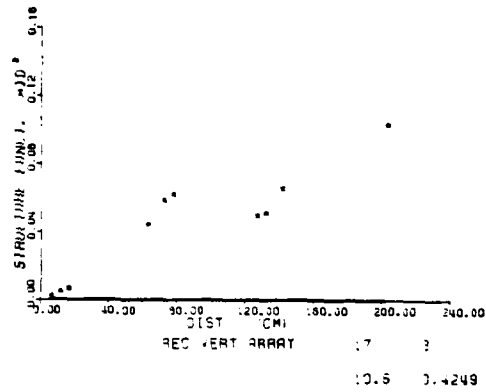
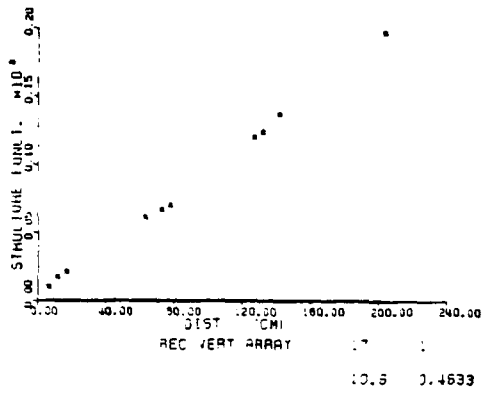


Figure 18. Vertical array structure functions (top row) and autocorrelation functions (second row), and horizontal array structure functions (third row) and autocorrelation functions (bottom row) for 0100 (left column) and 0300 (right column), 17 August.

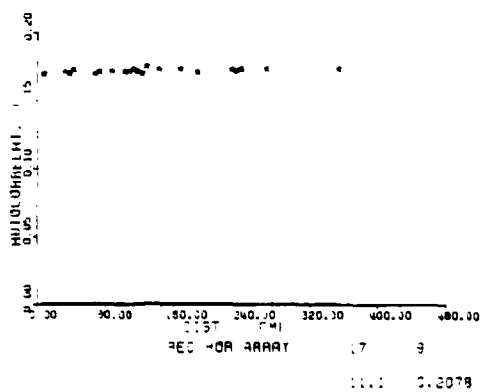
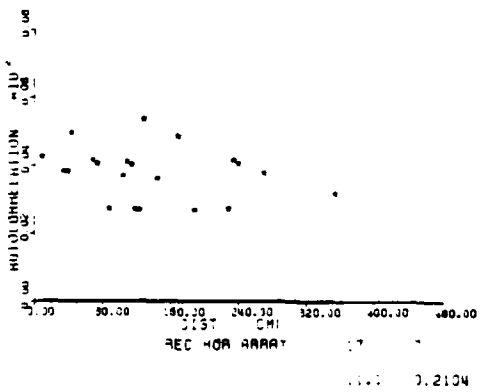
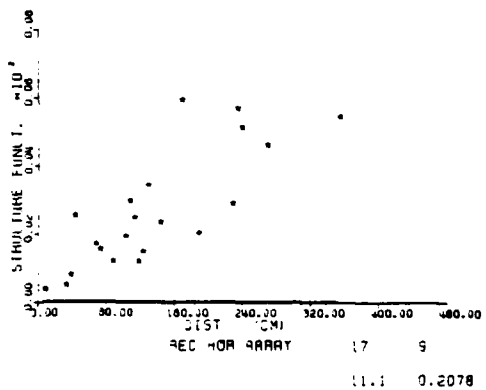
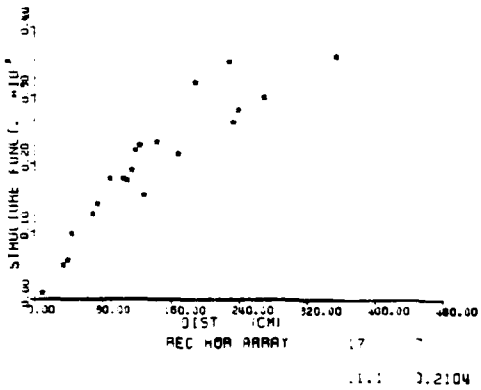
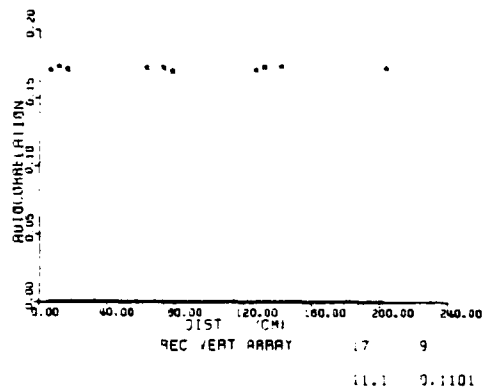
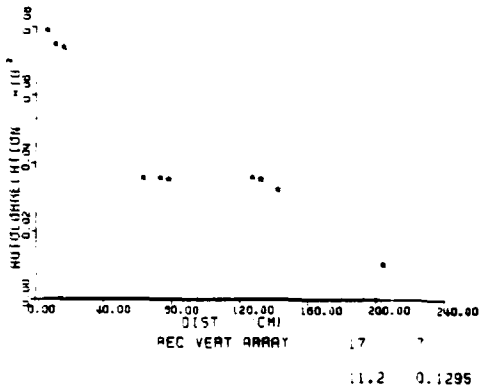
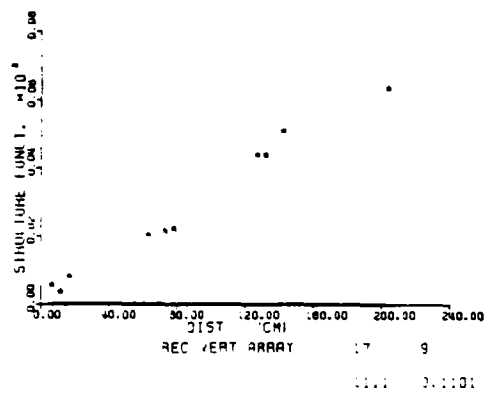
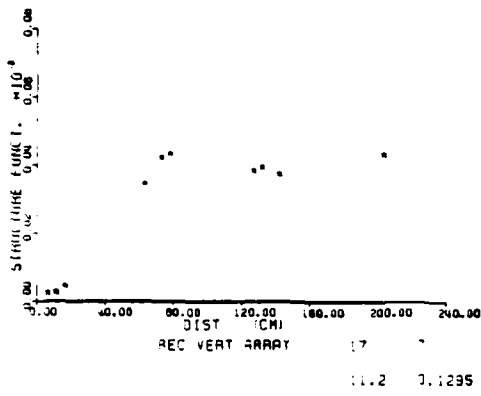


Figure 19. Vertical array structure functions (top row) and autocorrelation functions (second row), and horizontal array structure functions (third row) and autocorrelation functions (bottom row) for 0700 (left column) and 0900 (right column), 17 August.

When the array was too short, for example at 0100, the measured autocorrelation functions were linearly extrapolated to a zero-crossing. The integral scale is a relatively rough measure and is not very sensitive to the extrapolation procedure.

The Taylor micro-scale can also be calculated by assuming the micro-scale is quasi-Gaussian, where the autocorrelation function is described by

$$R_x(\rho) = R_x(\phi) e^{-\beta^2 \rho^2} \quad (22)$$

where  $\beta$  is a decay constant.

The microscale,  $M$ , for a turbulent medium is defined by fitting a parabola to the smallest scales and measuring the zero-cross, and is given by

$$\left. \frac{\frac{d^2 R_x(\rho)}{d\rho^2}}{R_x(\phi)} \right|_{\rho \rightarrow 0} = \frac{-2}{M^2} \quad (23)$$

For a process described by (23),

$$M = 1.12 \lambda \quad (24)$$

Examining first the examples of the vertical array autocorrelation functions, at 0100, the integral scale length was  $\lambda = 570\text{cm}$ ; at 0300, the correlation length decreased to  $\lambda = 152\text{cm}$ ,  $\lambda = 230\text{cm}$  at 0700, and  $\lambda$  very large at 0900. The

horizontal array correlation lengths were always greater, with  $\lambda = 760\text{cm}$  at 0100,  $\lambda$  very large at 0300,  $\lambda = 1,560\text{cm}$  at 0700, and  $\lambda = 860\text{cm}$  at 0900. The integral scales for the vertical and horizontal arrays for the four days are plotted later (Figures 25 and 26). The integral scales varied considerably with time. The anisotropy of the vertical to horizontal scales is evident, but not very strong, with the average  $\lambda$  (horizontal)/ $\lambda$  (vertical)  $\approx 4$ .

Five examples of half-hour time series of pulse travel time are shown in Figure 20. Each plot contains three hundred travel-time estimates calculated from the digitized hydrophone signal, and examples have been selected from August 16, hours 0100, 0300, 0500, 0700 and 1900. The travel time plots are automatically scaled to show details of the variations, and have arbitrary, but fixed, mean offsets for each channel. These plots consistently show slow and relatively smooth changes in the acoustic travel time, with fluctuation periods of the same order as the half-hour sample period. In periods of low activity, such as Figure 20, the scatter of the one microsecond measurement resolution steps can be seen, suggesting that the rms noise of the travel time estimates is approximately one microsecond. The standard deviation of the travel time fluctuations were calculated for each half hour sample between August 16 and 18, and were found to range between 1 and  $60\mu\text{s}$  for both hydrophones. These standard deviation estimates are plotted in Figure 21. It is clear

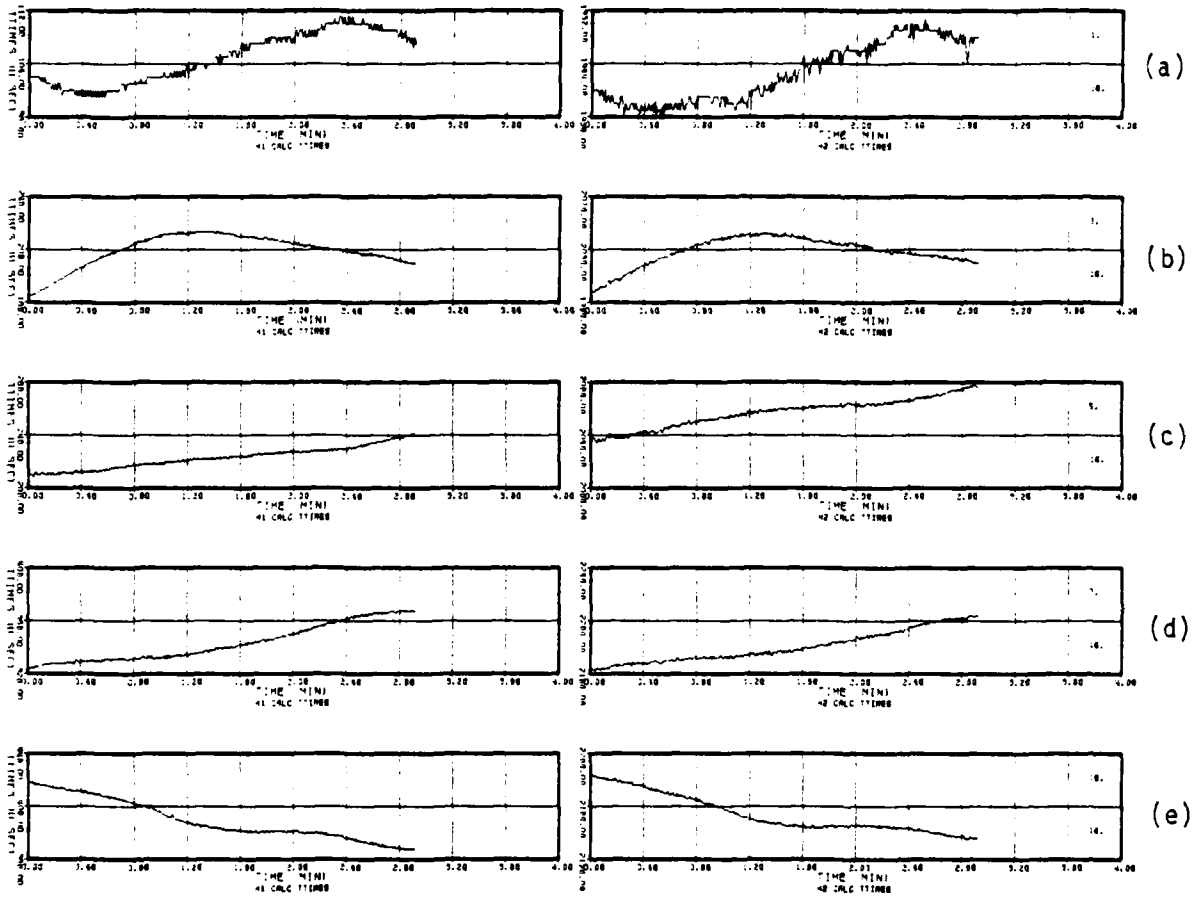


Figure 20. Travel-time estimates for 16 August:

- a) Hour 0100
- b) Hour 0300
- c) Hour 0500
- d) Hour 0700
- e) Hour 1900

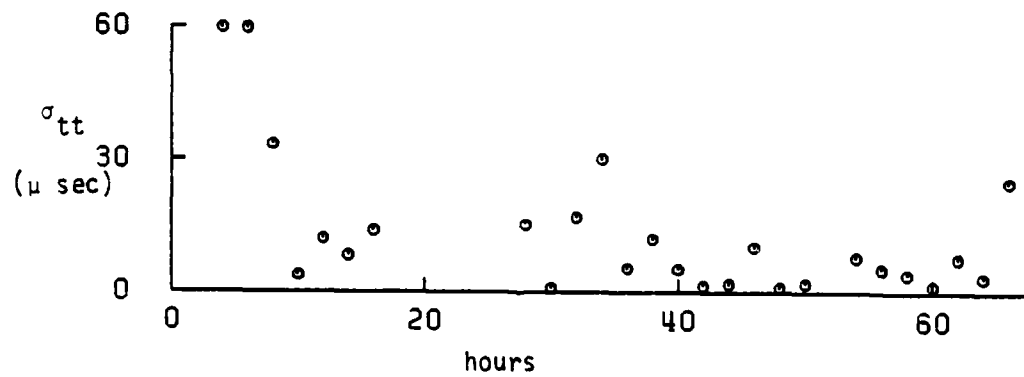
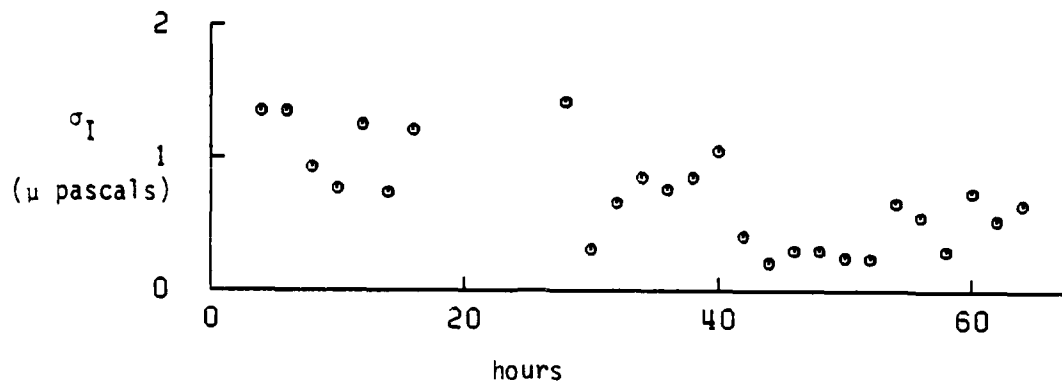


Figure 21. Time-series of standard deviations of travel-time (lower panel) and pulse amplitude (upper panel) for 16-18 August.

from the scatter of the points that there are large changes in the variability of sound-speed propagation across the Canyon between each half-hour sampling period. Some of this scatter in the standard deviation estimates is due to under-sampling of partially periodic travel time fluctuations, but inspection of other time-series in the four-day sample show long quiescent periods followed by bursts of high sound-speed variations.

The corresponding 20 KHz pulse amplitude time-series are shown in Figure 22. The most significant differences between the travel-time and amplitude data are more rapid fluctuations in the amplitude signal. Additionally, there were significant differences in the amplitude received by the two hydrophones, which were separated by only 2m; this suggests that the intensity fluctuations are caused by refractive index fluctuations with scales much shorter than those associated with integral sound-speed variations recorded in the travel time measurement. Flatte (1979) has suggested that small changes of the geometry in the sound speed fluctuations along the acoustic ray path cause focusing and defocusing of the rays which are seen as large intensity variations at the receiver. The measurements of rapidly changing intensity made in this experiment support this hypothesis.

To examine the relationship between travel time and amplitude variations, a correlation plot was constructed (Figure 23). Despite the large scatter, the correlation

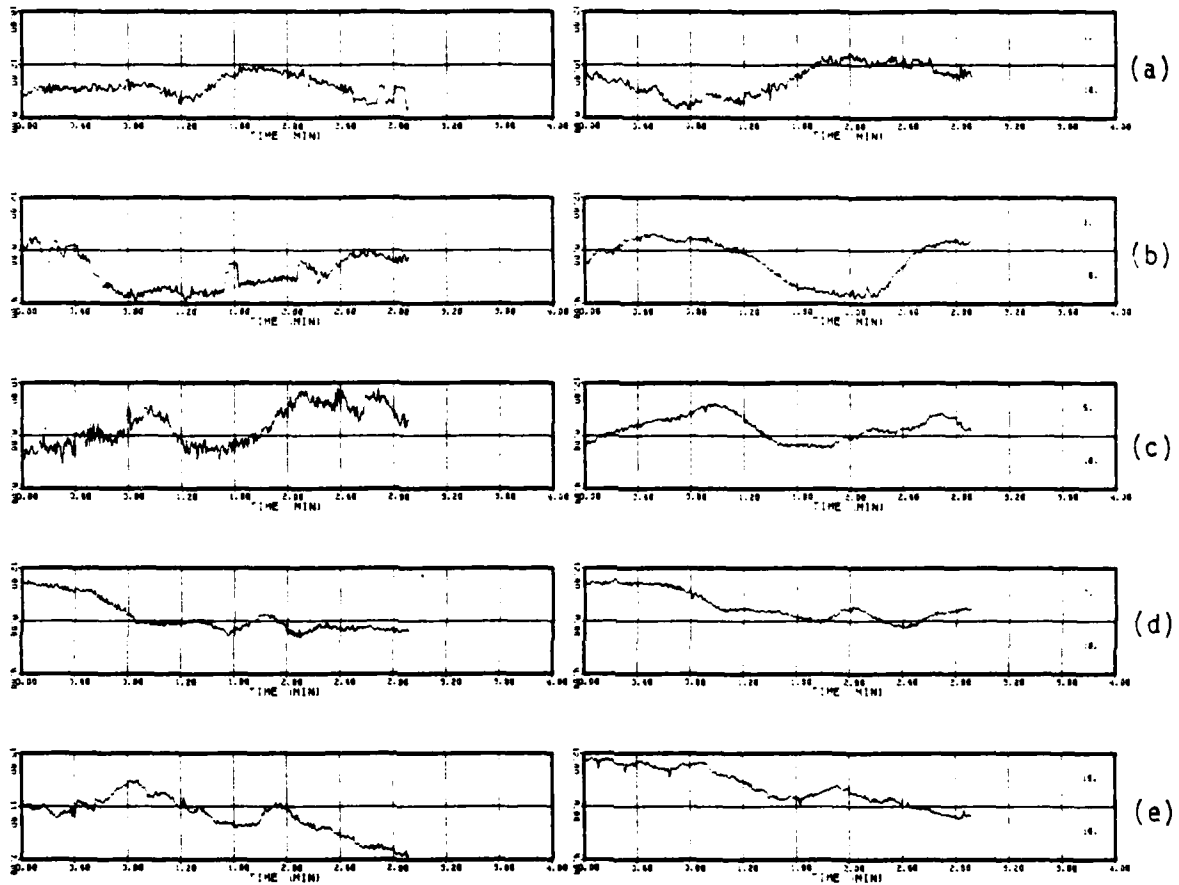


Figure 22. 20KHz pulse amplitude for 16 August:

- a) Hour 0100
- b) Hour 0300
- c) Hour 0500
- d) Hour 0700
- e) Hour 1900

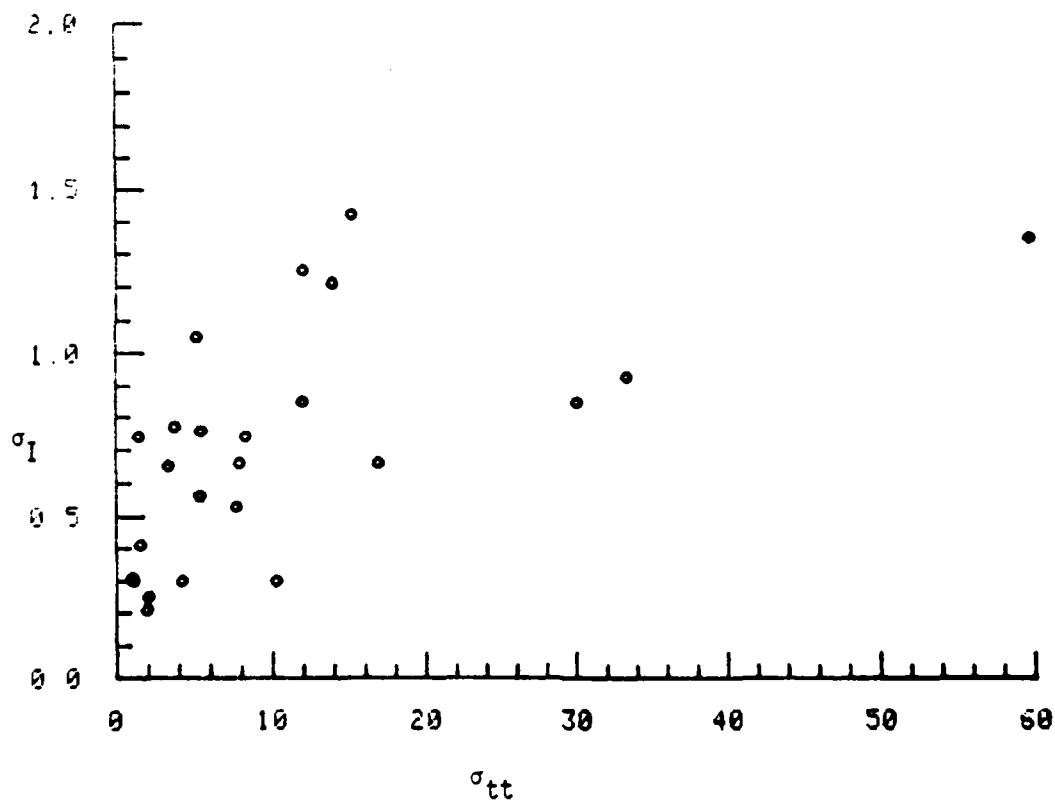


Figure 23. Correlation plot of travel-time,  $\sigma_{tt}$ , and pulse amplitude,  $\sigma_I$ , standard deviations.

plot does suggest that, while large intensity fluctuations occurred without large integral sound-speed variations, the converse is not true, i.e., large intensity fluctuations occurred in periods with minimal travel time changes.

To place the AVEK results in Flatte's strength/diffraction space (see equations 18 and 20) the values of  $\phi$  and  $\Lambda$  were calculated from the correlation lengths measured at the receiver array for an acoustic frequency of 20 KHz. These estimates are plotted in Figures 24 and 25, using correlation lengths measured at the vertical and horizontal thermistor arrays, respectively. Although equations 18 and 20 do not strictly apply in the anisotropic conditions found at the AVEK site, the very low propagation angle (due to source and receiver being at the same depth  $\pm 2\text{m}$ ) allows us to assume isotropic conditions (see e.g., Desaubie, 1979). Even though the horizontal and vertical scales differ significantly, the points plotted in Figures 24 and 25 show the approximate position in the  $\phi$ - $\Lambda$  space of each half hour acoustic measurement. With two exceptions, all the points lie well within the geometrical optics regime.

The relationship between the temperature lengths scales, temperature variance, and the acoustic pulse amplitude may be seen in the time-series plotted in Figure 26. These plots fail to suggest any obvious relationship between the variables, but does show the large aperiodic fluctuations over the sixty-hour sample interval. A similar set of time-series including travel-time standard deviations is shown in Figure

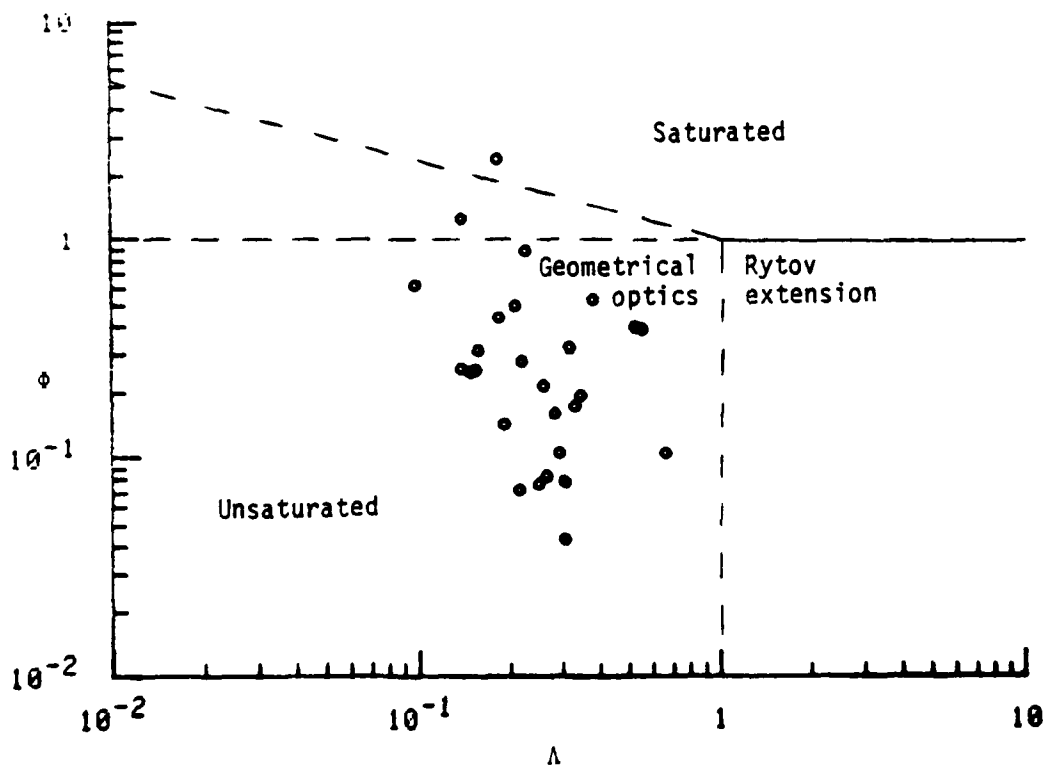


Figure 24. Strength,  $\phi$ , versus diffraction,  $\Lambda$ , for 16-18 August, using vertical length scales measured at the receiver tripod.

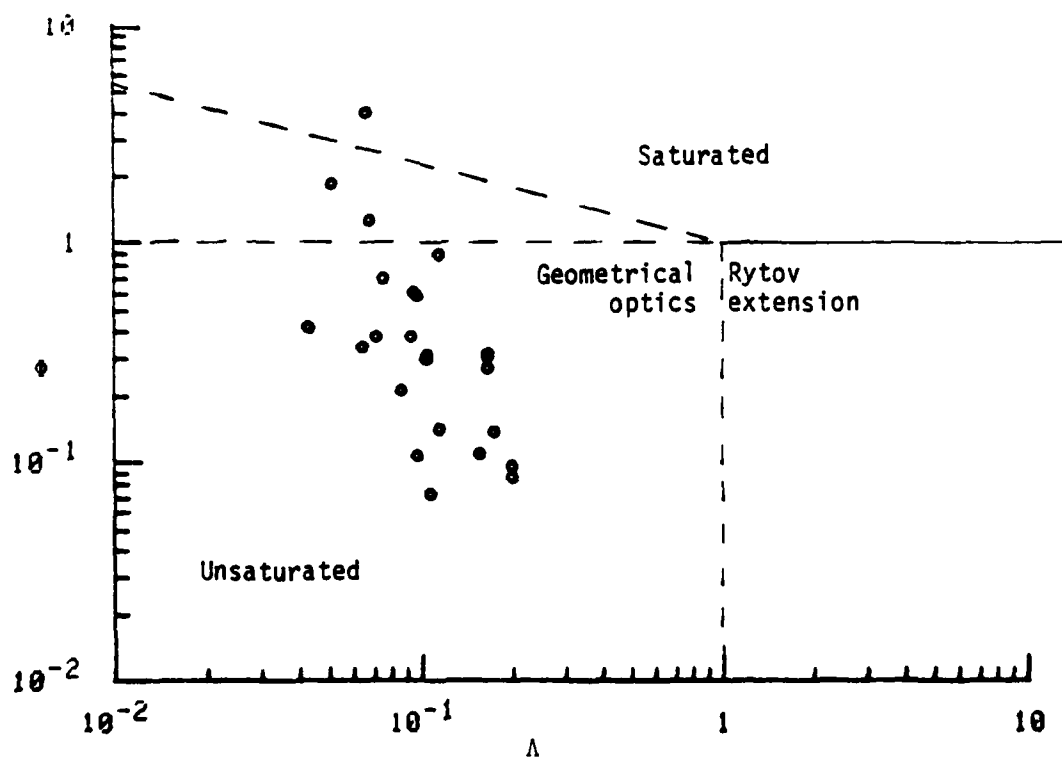


Figure 25. Strength,  $\phi$ , versus diffraction,  $\Lambda$ , for 16-18 August, using horizontal length scales measured at the receiver tripod.

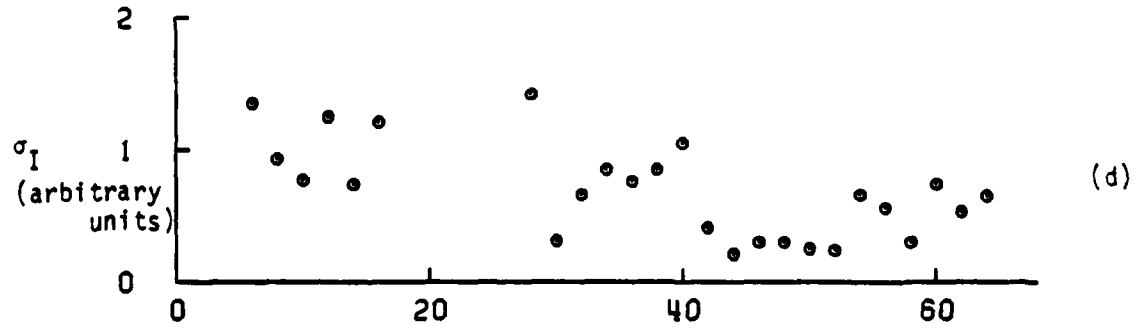
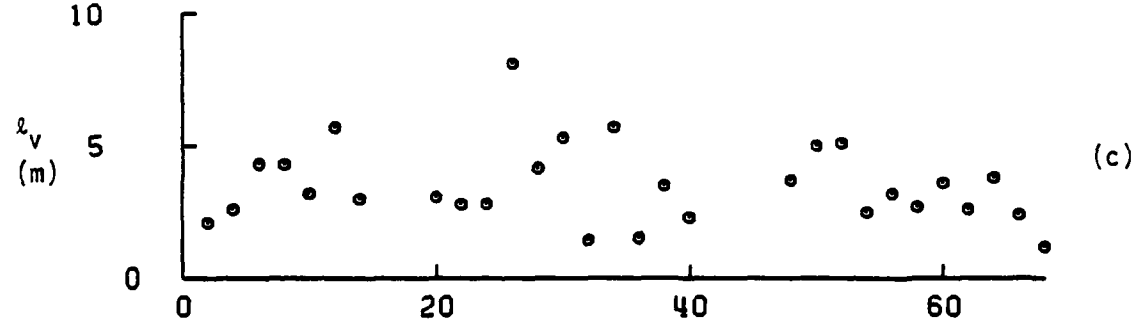
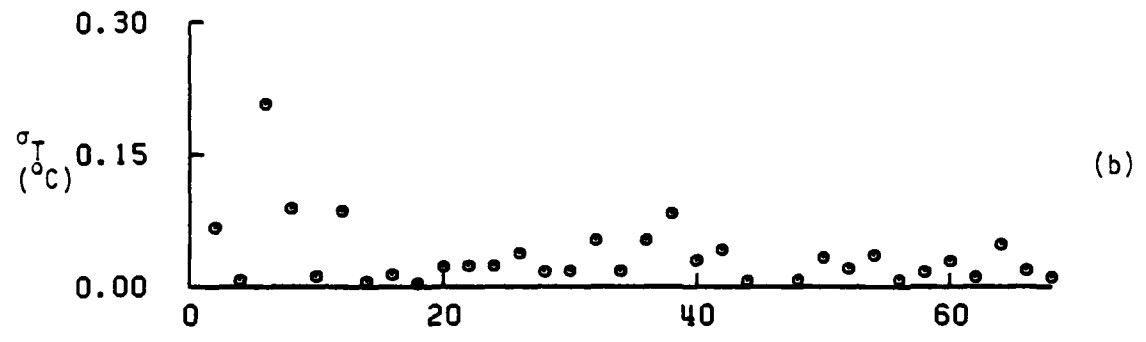
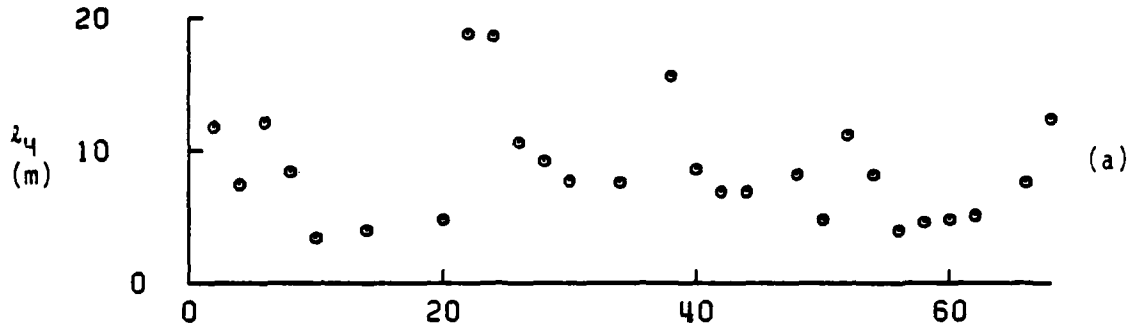


Figure 26. a) Horizontal integral scale(m) vs. time(hours),  
 b) Temperature standard deviation( $^{\circ}$ C) vs. time(hours),  
 c) Vertical integral scale(m) vs. time(hours),  
 d) Amplitude standard deviation(arbitrary units).

27. Again the large variations of the travel-time can be seen.

To test whether a causal relationship exists between the measured temperature scales and variance, correlation plots using Chernov's criteria and the Debye Approximation were made. In Figure 28, pulse amplitude is plotted against  $\sigma_T \ell_H^{-3/2}$  where  $\sigma_T$  is the temperature standard deviation and  $\ell_H$  is the horizontal integral scale length, to test Chernov's formula for amplitude variance (equation 12). The large scatter in this plot indicates that the relationship is not confirmed for these measurements.

A similarly poor correlation was obtained when amplitude variation was plotted against  $\sigma_T \sqrt{\ell_H}$  (see Figure 29) to test the Debye approximation (equation 16).

The reason for the very large scatter in these correlation plots is probably that both the length-scales and temperature variances measured at the receiver tower were not always typical of the temperature field along the entire transmission path. (The failure of the yo-yo profiler, which was to have provided the principle temperature structure data at about mid-range, prevents better estimates of the refractive index field.)

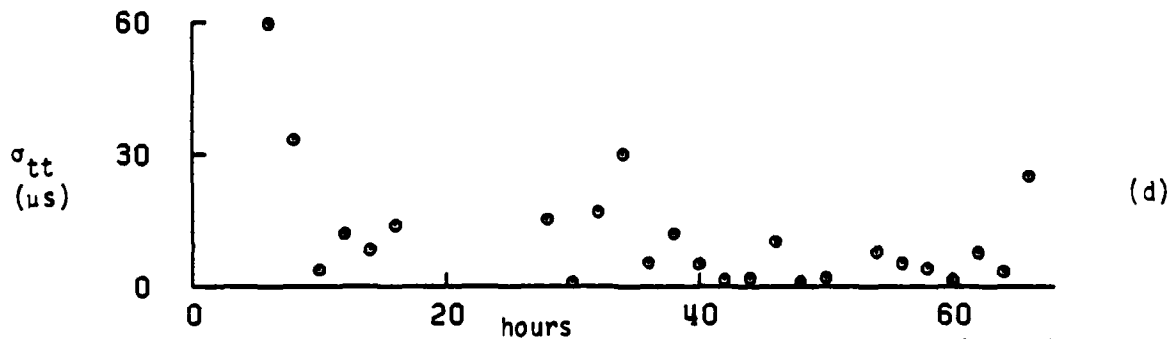
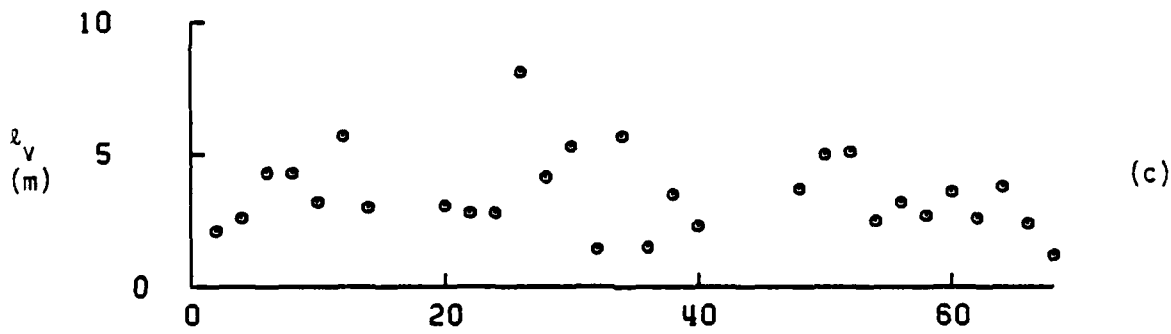
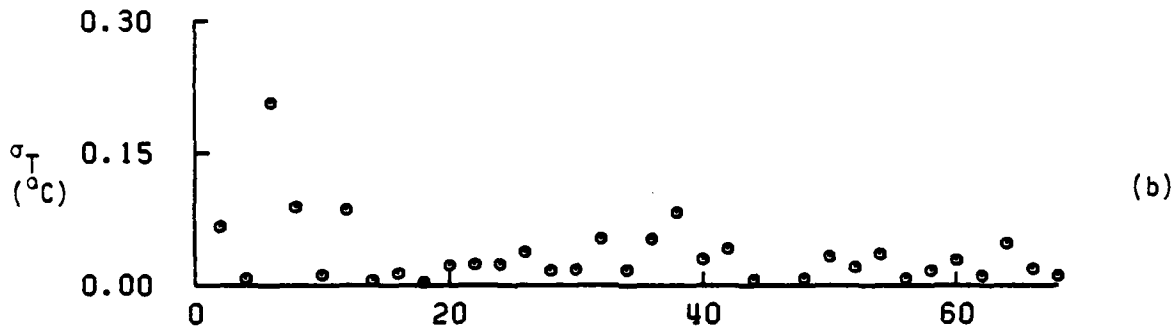
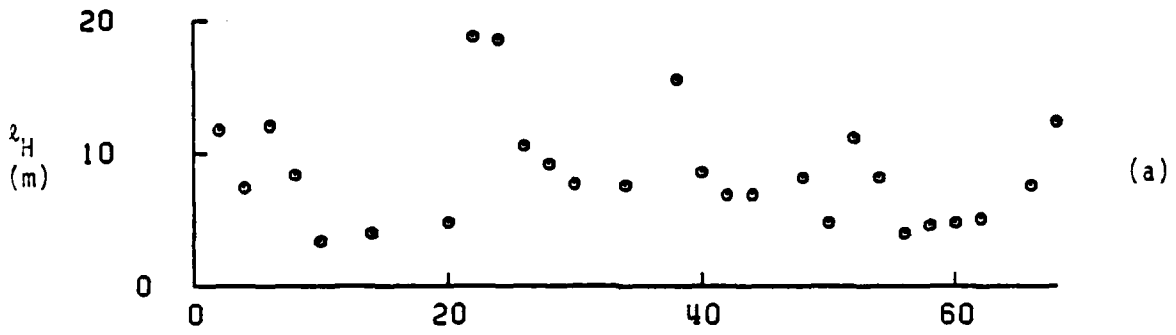


Figure 27. a) Horizontal integral scale(m) vs. time(hours),  
 b) Temperature standard deviation( $^{\circ}$ C) vs. time(hours),  
 c) Vertical length-scale(m) vs. time (all measured at the receiver array),  
 d) Travel-time standard deviation( $\mu$ s).

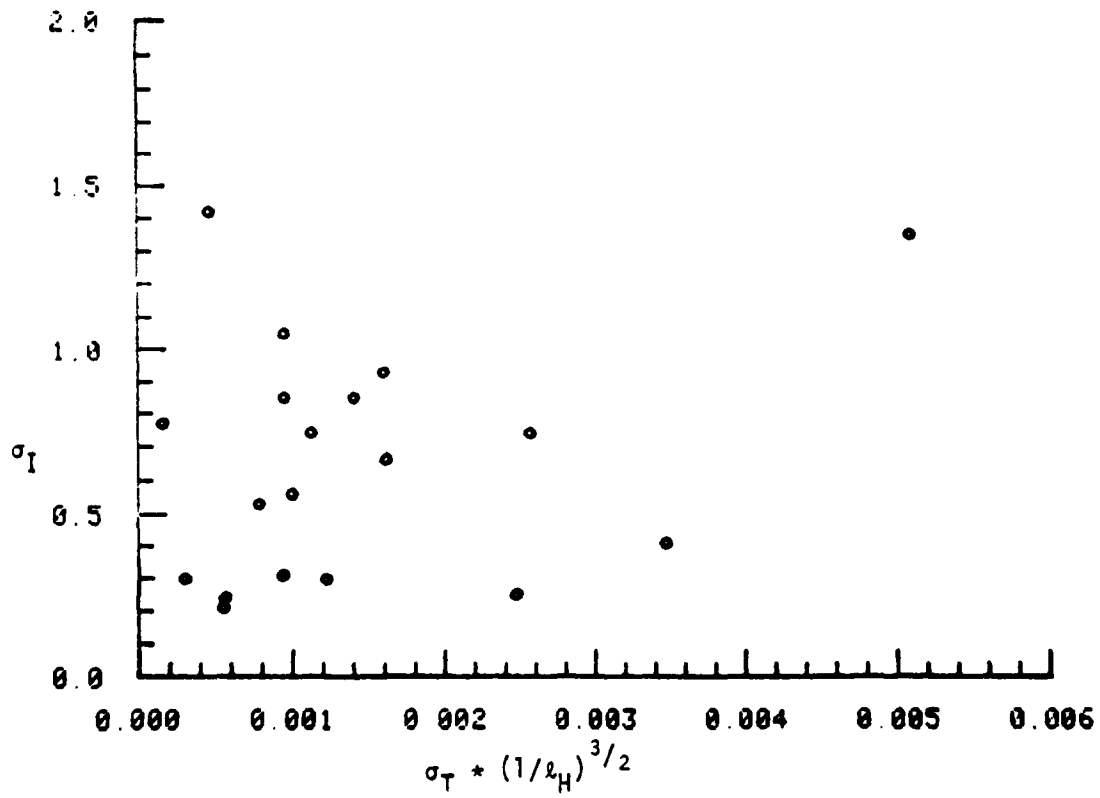


Figure 28. Correlation between amplitude variations, length-scales, and temperature variance using Chernov's model (arbitrary units).

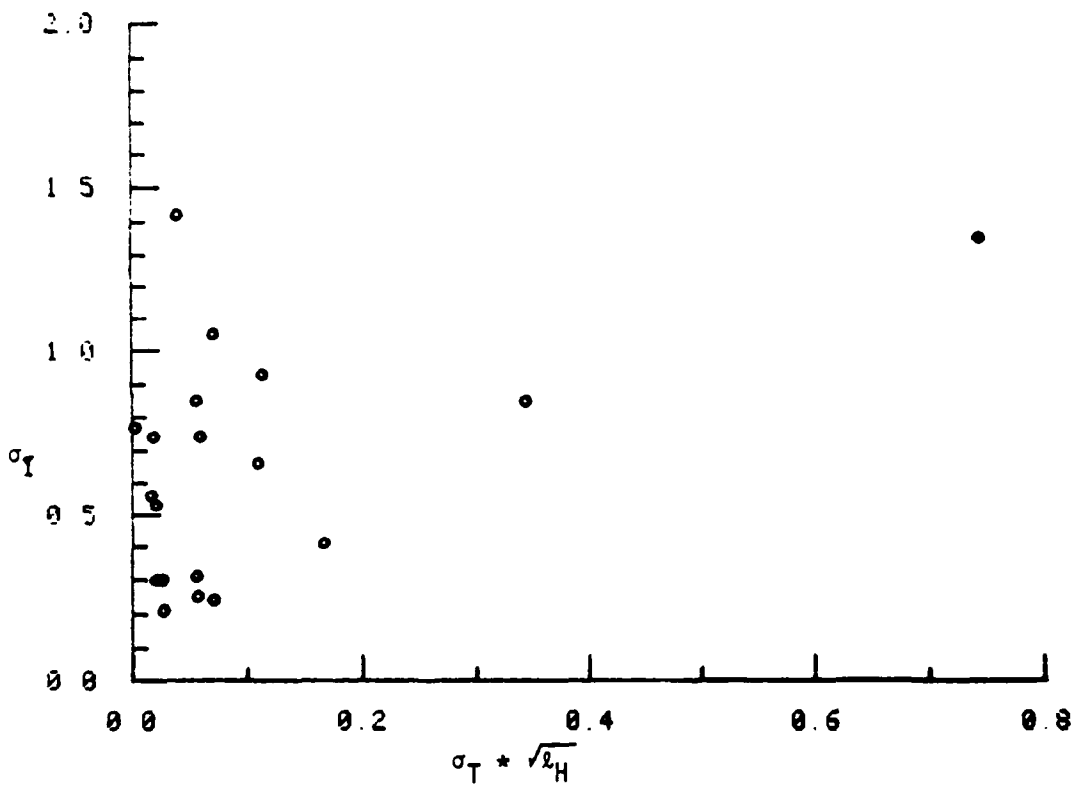


Figure 29. Correlation between amplitude variations, length-scales, and temperature variance using the Debye approximation (arbitrary units).

## V. SUMMARY AND CONCLUSIONS

The Acoustic Variability Experiment (AVEX) described here measured acoustic pulse propagation along a wholly refracted 400m path between a fixed source and receiver in the upper ocean. The acoustic pulse was composed of a 0.5ms burst of 20 KHz CW followed by a 4.5ms pseudo random noise pulse containing energy in the frequency range between 5 and 25 KHz. The source and receivers were stably mounted on towers located on each side of Carmel Canyon at a depth of 30m.

The temporal variability of acoustic amplitude and phase was measured and a preliminary analysis of the 20 KHz pulse data has been described. The travel time across the Canyon had rms variations between 1 and 60 $\mu$ s, calculated over each half-hour sample period, and corresponding 20 KHz pulse amplitude fluctuations between 3% and 14%. The level of these fluctuations changed dramatically in the 1.5 hours between successive measurements.

Both the temporal and spatial structure of the temperature field were measured simultaneously with the acoustic transmission at the source, receiver and at a mid-point. A spectrum of a 15-day temperature record showed the large scale variability due to inertial and tidal motions and to internal waves at higher frequencies. The microstructure was intermittent and appeared to be associated with the internal waves. The temperature integral scales calculated

from the spatial autocorrelation functions ranged from 1.2 to 14m (est) in the vertical and from 3.4m to greater than 50m (est) in the horizontal. The temperature structure was anisotropic with the average horizontal to vertical scale ratio equal to about four.

An attempt to compare the measured acoustic amplitude variance with temperature scale lengths and variance using the theoretical predictions of Chernov and Debye failed to show any consistent relationship. These tests showed that poor correlations existed between acoustic intensity and the temperature structure measured at the side of the Canyon by the receiver thermistor arrays. Due to the failure of the yo-yo profiler, more representative measurements of the temperature structure along the propagation path were not available. The experiment did demonstrate the highly episodic character of the finestructure in the Canyon temperature field, which appeared to be dominated by internal wave activity. The intermittent bursts of activity were reflected in both the thermistor array temperature measurements, and indirectly by the pulse intensity and travel-time estimates.

### LIST OF REFERENCES

- Batchelor, G.K., 1947, "Kolmogorov's Theory of Locally Isotropic Turbulence", Proc. Camb. Phil. Soc. 43, p. 533.
- Chernov, L.A., 1960, Wave Propagation in a Random Medium, translated by R.A. Silverman, McGraw-Hill.
- Clark, J.G., and M. Kronengold, 1976, "Long-period Fluctuations of CW Signals in Deep and Shallow Water". J. Acoust. Soc. Am. 56, 1071-83.
- Crawford, W.R., and Osborn, T.R., 1980, "Microstructure Measurements in the Atlantic Equatorial Undercurrent During GATE". Deep-Sea Research 26 (supp. 1979).
- Ewart, T.E., 1976, "Acoustic Fluctuations in the Open Ocean-- A Measurement using a Fixed Refracted Path", J. Acoustic Society of America 60, p. 46-59.
- Fedorov, K.N., 1978, The Thermohaline Finestructure of the Ocean, D.A. Brown, translator, J.S. Turner, tech. ed., Pergamon Press, Oxford, 170 pp.
- Flatte, S.M., 1979, Sound Transmission through a Fluctuating Ocean, Cambridge Univ. Press, 291 pages.
- Gargett, A.E. and T.R. Osborn, 1981, "Small-Scale Shear Measurements During Fine and Microstructure Experiment (Fame)", J. Geophys. Res., 86, C3, p. 1929-1944.
- Garrett, C.J.R., and W.H. Munk, 1972. "Space-time Scales of Internal Waves", Geophysical Fluid Dynamics 3: 225-264.
- Garrett, C.J.R. and W.H. Munk, 1975. "Space-time Scales of Internal Waves: A Progress Report". Journal of Geophysical Research 80: 291-297.
- Garrett, C.J.R., and W. Munk, 1979. "Internal Waves in the Ocean". Annual Review of Fluid Mechanics 11: 339-369.
- Gibson, C.H., 1980. "Fossil Temperature, Salinity, and Vorticity Turbulence". In: Marine Turbulence, J.C.J. Nihoul, ed., Elsevier, Amsterdam.
- Grant, H.L., R.W. Stewart, and A. Moilliet, 1962. "Turbulence Spectra from a Tidal Channel". Journal of Fluid Mechanics 12: 241-268.

- Kennedy, R.M., 1960, "Phase and Amplitude Fluctuations in Propagating Through a Layered Ocean", Journal of the Acoustical Society of America, 46, p. 737-745.
- Kolmogorov, A.N., 1941, "Local Structure of Turbulence in an Incompressible Fluid at Very High Reynolds Numbers", Doklady AN SSSR, 30 (4), p. 299-303.
- Liebermann, L., 1951, "The Effect of Temperature Inhomogeneities in the Ocean on Propagation of Sound", Journal of the Acoustical Society of America, 23 (5), p. 563-570.
- Levine, M.D. and J.R. Irish, 1981, "A Statistical Description of Temperature Finestructure in the Presence of Internal Waves", Journal of Physical Oceanography 11, no. 5, p. 676-691.
- Mintzer, D., "Wave Propagation in a Randomly Inhomogeneous Medium", Journal of the Acoustical Society of America, 25 Part I, p. 922-927; Part II, 1107-1111, 1953; and 206 (2) Part III, 186-190, March 1954.
- Munk, W., 1981, "Internal Waves and Small-Scale Processes", In: Evolution of Physical Oceanography, edited by B.A. Warren and C. Wunsch, MIT Press, Cambridge, MA. 623 pp.
- Nuebert, J.A., 1970, "Asymptotic Solution of the Stochastic Helmholtz Equation for Turbulent Water", Journal of the Acoustical Society of America, 48(5), Part 2, p. 1203-1211.
- Phillips, O.M., 1977, The Dynamics of the Upper Ocean, Cambridge University Press, 2nd ed., 276 pages.
- Porter, R.P., R.C. Spindel, and R.J. Jaffee, 1977, "Acoustic Internal Wave Interaction at Longranges in the Ocean", Journal Acoustic Soc. Am. 56, 1426-1436.
- Rytov, S.M., 1937, "Diffraction of Light By Ultrasonic Waves", Izv. Akol. Nauk SSSR, Ser. Fiz., 2, p. 233.
- Sagar, F.H., 1955, "Fluctuations in Intensity of Short Pulses of 14.5-Kc Sound Received from a Source at Sea", Journal of the Acoustical Society of America, 27 (6), p. 1092-1106.
- Sagar, F.H., 1957, "Comparison of Experimental Underwater Acoustic Intensities of Frequency 14.5-Kc with Values Computed for Selected Thermal Conditions at Sea", Journal of the Acoustical Society of America, 29 (8), p. 948-965.
- Sagar, F.H., 1960, "Acoustic Intensity Fluctuations and Temperature Microstructure in the Sea", Journal of the Acoustical Society of America, 32 (1), p. 112-121.

- Sheehy, M.J., 1950, "Transmission of 24 KHz Sound From a Deep Source", Journal of the Acoustical Society of America, 22, (1), p. 24-28.
- Stone, R.G., and D. Mintzer, 1962, "Range Dependence of Acoustic Fluctuations in a Randomly Inhomogeneous Medium", Journal of the Acoustical Society of America, 34, p. 647-653.
- Stone, R.G., and D. Mintzer, 1965, "Transition Regime for Acoustic Fluctuations in a Randomly Inhomogeneous Medium", Journal of the Acoustical Society of America, 38, p. 843-846.
- Steinberg, J.C., J.G. Clark, H.A. DeFerrari, J. Kronengold, and K. Yacoub, 1971, "Fixed-system Studies of Underwater-Acoustic Propagation", J. Acoust. Soc. Am. 52, 1521-1535.
- Tatarski, V.I., 1961, Wave Propagation in a Turbulent Medium, translated by R.A. Silverman, McGraw-Hill.
- Turner, J.S., 1981, "Small-scale Mixing Processes", In: Evolution of Physical Oceanography, edited by B.A. Warren and C. Wunsch, MIT Press, Cambridge, MA. 623 pp.
- Woods, J.D., 1968, "Wave-induced Shear Instability in the Summer Thermocline", Journal of Fluid Mechanics 32: 791-800.
- Zenk, W., and E.J. Katz, 1975, "On the Stationarity of Temperature Spectra at High Horizontal Wave Numbers", J. of Geophysical Research 80, 27. P. 3885-3891.

INITIAL DISTRIBUTION LIST

	No. Copies
1. Defense Technical Information Center Cameron Station Alexandria, VA 22314	2
2. Library, Code 0142 Naval Postgraduate School Monterey, CA 93940	2
3. Chairman (Code 68Mr) Department of Oceanography Naval Postgraduate School Monterey, CA 93940	1
4. Chairman (Code 63Rd) Department of Meteorology Naval Postgraduate School Monterey, CA 93940	1
5. Prof. E.B. Thornton, Code 68Tm Naval Postgraduate School Monterey, CA 93940	5
6. Director Naval Oceanography Division Naval Observatory 34th and Massachusetts Avenue NW Washington, D.C. 20390	1
7. Commander Naval Oceanography Command NSTL Station Bay St. Louis, MS 39522	1
8. Commanding Officer Naval Oceanographic Office NSTL Station Bay St. Louis, MS 39522	1
9. Commanding Officer Fleet Numerical Oceanography Center Monterey, CA 93940	1
10. Commanding Officer Naval Ocean Research and Development Activity NSTL Station Bay St. Louis, MS 39522	1

11. Commanding Officer 1  
 Naval Environmental Prediction  
 Research Facility  
 Monterey, CA 93940
12. Chairman, Oceanography Department 1  
 U.S. Naval Academy  
 Annapolis, MD 21402
13. Chief of Naval Research 1  
 800 N. Quincy Street  
 Arlington, VA 22217
14. Office of Naval Research (Code 480) 1  
 Naval Ocean Research and Develop-  
 ment Activity  
 NSTL Station  
 Bay St. Louis, MS 39522
15. Scientific Liaison Office 1  
 Office of Naval Research  
 Scripps Institution of Oceanography  
 La Jolla, CA 92037
16. Library 1  
 Scripps Institution of Oceanography  
 P.O. Box 2367  
 La Jolla, CA 92037
17. Library 1  
 Department of Oceanography  
 University of Washington  
 Seattle, WA 98105
18. Library 1  
 School of Oceanography  
 Oregon State University  
 Corvallis, OR 97331
19. Commander 1  
 Oceanographic Systems Pacific  
 Box 1390  
 Pearl Harbor, HI 96860
20. Commanding Officer 2  
 Naval Oceanography Command Center, Guam  
 Box 12  
 Fleet Post Office  
 San Francisco, CA 96630
21. LCDR Mark Wakeman 2  
 Naval Oceanography Command Center, Rota  
 Box 31  
 Fleet Post Office  
 New York, NY 09540

END

DATE  
FILMED

4-82

DTIC